NASA Public Access
Author manuscript
Meteorit Planet Sci. Author manuscript; available in PMC 2020 April 03.

Published in final edited form as:
Meteorit Planet Sci. 2019 September 1; 54(9): 2046–2066. doi:10.1111/maps.13348.

Using dust shed from asteroids as microsamples to link remote measurements with meteorite classes

B. A. COHEN[1,*], **J. R. SZALAY**[2], **A. S. RIVKIN**[3], **J. A. RICHARDSON**[1], **R. L. KLIMA**[3], **C. M. ERNST**[3], **N. L. CHABOT**[3], **Z. STERNOVSKY**[4,5], **M. HORÁNYI**[4,6]

[1]NASA Goddard Space Flight Center, Greenbelt, Maryland 20771, USA

[2]Princeton University, Princeton, New Jersey 08544, USA

[3]Applied Physics Laboratory, Johns Hopkins University, Laurel, Maryland 20723, USA

[4]LASP, University of Colorado, Boulder, Colorado 80303, USA

[5]Smead Aerospace Sciences, University of Colorado, Boulder, Colorado 80309, USA

[6]Physics Department, University of Colorado, Boulder, Colorado 80309, USA

Abstract

Given the compositional diversity of asteroids, and their distribution in space, it is impossible to consider returning samples from each one to establish their origin. However, the velocity and molecular composition of primary minerals, hydrated silicates, and organic materials can be determined by in situ dust detector instruments. Such instruments could sample the cloud of micrometer-scale particles shed by asteroids to provide direct links to known meteorite groups without returning the samples to terrestrial laboratories. We extend models of the measured lunar dust cloud from LADEE to show that the abundance of detectable impact-generated microsamples around asteroids is a function of the parent body radius, heliocentric distance, flyby distance, and speed. We use Monte Carlo modeling to show that several tens to hundreds of particles, if randomly ejected and detected during a flyby, would be a sufficient number to classify the parent body as an ordinary chondrite, basaltic achondrite, or other class of meteorite. Encountering and measuring microsamples shed from near-Earth and Main Belt asteroids, coupled with complementary imaging and multispectral measurements, could accomplish a thorough characterization of small, airless bodies.

INTRODUCTION

By number, asteroids dominate the inventory of the inner solar system. Over half a million asteroids are known, and tens of thousands more are discovered each year. The asteroid population has members ranging from unaltered, primordial objects to remnants of

This is an open access article under the terms of the Creative Commons Attribution-NonCommercial License, which permits use, distribution and reproduction in any medium, provided the original work is properly cited and is not used for commercial purposes.
http://creativecommons.org/licenses/by-nc/4.0/

*Corresponding author. barbara.a.cohen@nasa.gov.

Editorial Handling—Dr. Donald Brownlee

NASA Author Manuscript
NASA Author Manuscript
NASA Author Manuscript

NASA Author Manuscript NASA Author Manuscript NASA Author Manuscript

differentiated parent bodies. Despite being composed mostly of silicate minerals, asteroids may have been important vectors for the delivery of water and organic materials to the early Earth (Morbidelli et al. 2000); recent measurements by the Rosetta spacecraft are inconsistent with a major cometary contribution (Altwegg et al. 2014) leaving asteroids as the likeliest exogenic contributor. Water or OH^-, bound into clay minerals, is present in amounts up to 10% or more by mass in carbonaceous chondrite meteorites (Brearley 2006) and many asteroid classes (Rivkin et al. 2002, 2013; Volquardsen et al. 2007). Organic material has been detected both in meteorites and Main Belt asteroids (Pizzarello et al. 2006; Campins et al. 2010; Rivkin and Emery 2010). Thus, asteroids are important targets for both scientific inquiries, addressing the NASA goal of exploring and observing the objects in the solar system to understand how they formed and evolved, and also for sustaining and expanding destinations for human exploration and resource utilization.

Telescopic observations are the primary tool for assessing the range of asteroid compositions and linking them to meteorites (Table 1) (Xu et al. 1995; Burbine and Binzel 2002; Bus and Binzel 2002; Reddy et al. 2015). The majority of these measurements focus on the 0.5–1.0 μm spectral range, which provides identification of major iron-bearing silicates, but only a small fraction of observations extends to the 2.5 μm region to capture robust measurements of a range of silicate, carbonate, and accessory mineral spectral features (Fig. 1). Focused observations integrating multiple wavelength regions are able to more effectively identify specific mineralogies, but the Earth's atmosphere severely limits many of these observations, including those of water and carbon-bearing materials. Compositions and meteorite linkages derived from telescopic spectra have been validated by spacecraft data to date for Eros, Itokawa, and Vesta (Veverka et al. 2000; Binzel et al. 2001; Fujiwara et al. 2006; Nesvorny et al. 2011; Reddy et al. 2013).

More definitive links between meteorites and asteroids may be made by analyzing samples of the parent body directly. The Hayabusa mission recovered thousands of sub-100 μm particles, linking the asteroid Itokawa to LL chondrites (Nesvorny et al. 2011). The Hayabusa 2 and OSIRIS-REx missions will collect more significant masses of regolith from asteroids to return to Earth for analysis (Lauretta et al. 2015; JAXA 2016). Sample return missions are costly and inevitably limited to a small number of asteroids. However, in-flight composition analysis of regolith microsamples shed from asteroid surfaces may present good alternatives to direct surface access by a lander (Krüger et al. 2003; Kempf 2009; Mann and Jessberger 2010; Postberg et al. 2011, 2014; Szalay and Horányi 2016c). In this paper, we investigate how well measurements made by dust analyzer instruments map to the chemical characteristics of meteorites, conduct statistical exercises to determine the number of particles required to tie such measurements to known meteorite groups, and model the dust cloud density around near-Earth and Main Belt asteroids to predict whether a sufficient number of particles could be encountered by a spacecraft-borne dust analyzer during asteroid flyby missions to confidently make this measurement.

IN SITU DUST PARTICLE ANALYSIS

Compositional analysis of dust particles encountered by spacecraft has been successfully conducted using dust detector instruments coupled with an impact-ionization mass

NASA Author Manuscript NASA Author Manuscript NASA Author Manuscript

spectrometer. Planetary, interplanetary, and interstellar dust grains have been analyzed in situ by dust instruments onboard spacecraft such as Vega-1 and Vega-2 (Kissel and Krueger 1987; Dikov et al. 1989), Giotto (Kissel 1986; Kissel et al. 1986), Helios 1 (Grün et al. 1980; Altobelli et al. 2006), Stardust (Kissel et al. 2003, 2004), and Cassini (Srama et al. 2004; Altobelli et al. 2016). Individual particles' origin as planetary or interplanetary is determined from impact speed and direction.

The interpretation of impact mass spectra in terms of elemental ratios and mineralogy is aided by laboratory calibration measurements and remotely sensed data. Dust samples from relevant minerals or homogenous synthetic materials can be prepared and accelerated to typical flyby velocities using electrostatic dust accelerators, enabling laboratory calibration measurements that can be used to quantitatively interpret the mass spectra; corresponding mineralogy can be inferred from elemental ratios (Goldsworthy et al. 2003; Fiege et al. 2014; Hillier et al. 2014, 2018; Altobelli et al. 2016). Many organic compounds can also be identified and quantified even at trace abundances (~1 ppm) (Kempf et al. 2012; Postberg et al. 2018).

As an example of the utility of in situ particle analysis and its fidelity, take the case of measurements of the composition of cometary dust. Cosmic dust samples have been extensively analyzed in the laboratory (e.g., Brownlee 1985) to provide reference compositions for these particles, so these studies illustrate the parameters and precision needed to make the links between in situ and lab measurements. Jessberger (1999) summarizes the results from the PUMA-1 instrument on Vega-1 sent to Comet P/Halley, and Sekanina et al. (2001) summarize the results from this detector as well as those from PIA on Giotto and PUMA-2 on Vega-2; in total, these detectors measured more than 2500 individual grains using a mass spectrometer with mass resolution ~100. At the high velocity of these dust impacts (typically above 20 km s^{-1}), the grains were completely vaporized and yielded cation spectra easily interpreted as elemental (rather than molecular) ions. Using the elemental ratios of Mg, Fe, Si, C, and S, Fomenkova et al. (1992) classified 2000 grains as metals, sulfides, silicates, and carbonaceous (CHON) particles, and identified organic compounds, pureC grains, iron-rich oxides, and carbonates. The mineralogical composition of Halley dust was estimated to be >20% Mg-silicates, ≈10% Fe-sulfides, 1–2% Fe metal, and <1% Fe oxide, leading to the conclusion that most of the comet Halley dust particles have an overall chondritic composition along with minor phases inferred to have a secondary origin.

Another successful example of effective and informative in situ grain characterization comes from the analysis of interplanetary, interstellar, and planetary dust particles by the Cassini Cosmic Dust Analyzer (CDA). CDA consisted of a dust detector and time-of-flight impact mass spectrometer, with a mass resolution of 10–50 over a mass range of 1–190 amu (Srama et al. 2004). CDA returned two mass spectra of particles ~2–6 nm in size during its cruise phase to Jupiter, which consisted primarily of Fe, with possible Ni and Cr, indicating they were composed of iron or kamacite (Hillier et al. 2007). Cassini encountered and characterized a further 36 grains classified as interstellar dust particles based on their high entry speed and direction. Their major elemental ratios (Mg/Si, Fe/Si, Mg/Fe, and Ca/Fe) were interpreted as representing magnesium-rich grains of silicates, oxides, and Fe-Ni metal

NASA Author Manuscript NASA Author Manuscript NASA Author Manuscript

in ratios consistent with CI chondrites (Altobelli et al. 2016). At Saturn, the CDA recorded thousands of mass spectra of E-ring particles derived from Saturn's moon Enceladus (Spahn et al. 2006). These particles have radii of 0.1–1 mm and are composed of water ice, water ice with significant organic and/or siliceous material, and water ice particles with particularly high sodium contents, providing evidence for a subsurface ocean on Enceladus in contact with a silicate seafloor (Postberg et al. 2009). CDA also observed silica particles <10 nm in size that were originally embedded in the icy particles, interpreted to be products of alkaline hydrothermal activity at the bottom of such an ocean (Hsu et al. 2015).

LINKING INDIVIDUAL PARTICLE COMPOSITION TO METEORITES

The examples of grain analysis from cometary tails, interstellar dust, and E-ring particles are examples of multiple detections of particles from a relatively well-known and homogeneous source. Asteroids, and their meteorite building blocks, are diverse in their chemical and mineralogic makeup, reflecting the range of parent bodies and geologic evolution of the solar system. In this section, we consider whether compositional information obtained on individual particles shed from asteroids can effectively to link them to known meteorite groups. We consider a simple case, where an asteroid's surface is made of a single meteorite type, and is shedding unaltered, monomineralic particles for detection by a flyby instrument. In the discussion, we will consider adjustments to the simple case based on observations from current spacecraft.

In the laboratory, meteorites are classified using petrologic characteristics (e.g., texture, mineralogy), elemental composition, and isotopic composition, and classification ranges from iron and nickel metals from protoplanetary cores to primitive stony meteorites that have never been significantly heated, along with some meteorites that do not fit in existing groups. While these measurements are more complex than can be expected for dust analyzers, previous missions showed that estimates of major mineral abundance (silicates, oxides, sulfides, metal) and elemental ratios could be obtained at a level sufficient to classify particles as IDPs. This same combination of mineral abundance and mineral composition is also generally sufficient to classify a bulk sample within the major meteorite groups, that is, as an ordinary (H, L, LL) chondrite, carbonaceous (C) chondrite, enstatite (E) chondrite, Rumuruti (R) chondrite, basaltic achondrite (eucrite, diogenite, angrite, aubrite, ureilite), primitive achondrite (brachinite, acapulcoite, lodranite, winonaite), or metal-rich achondrite (mesosiderite, pallasite, iron) (Rubin 1997). To illustrate this, we used compilations of published point-counts to compile the average abundance of silicates, oxides, sulfides, metal, and the Fe/Mg ratio in silicates in meteorite groups (Table 1) (Keil 1962, 1968, 2012; Buseck 1977; Bowman et al. 1996; Kallemeyn et al. 1996; Mittlefehldt et al. 1998; Bischoff et al. 2000; Singletary and Grove 2003; Bland et al. 2004; Jambon et al. 2005; Weisberg et al. 2006; Rubin 2007; Mayne et al. 2009).

Figure 2 graphically shows two possible combinations of parameters, the fraction of silicate particles versus the Fe content in the silicates, and ternary composition of abundance of Fe-Ni metal, oxides, and sulfides + phosphates. Figure 3 provides another representation that simultaneously considers all parameters using agglomerative hierarchical clustering (AHC), an iterative classification method where each meteorite class is compared with each other

NASA Author Manuscript NASA Author Manuscript NASA Author Manuscript

class, and successively merged (or agglomerated) into clusters until all classes have been merged into a single cluster that contains all classes (AHC was performed using the XLStat package for Excel, selecting the Pearson correlation coefficient for similarity and unweighted pair-group average for aggregation). In general, Figs. 2 and 3 show that these parameters are sufficient to distinguish major groups of meteorites from each other, but also highlight where potential confusion may arise, requiring additional information to help distinguish the classes. However, it is highly unlikely that analysis of such microsamples would be the only aim of a space mission. Contextual clues provided by other observations of the parent body (e.g., imaging and multispectral/hyperspectral analysis) would initially narrow the possible interpretation space. For example, pallasites and enstatite chondrites appear similar to each other using only these parameters, whereas they would be easily distinguished in infrared spectroscopy. Additionally, several types of meteorites may be recognizable by the presence of unique minerals, for example: oldhamite ([Ca,Mg]S) in enstatite chondrites, graphite (C) in ureilites, hibonite and mellilite ($CaAl_{12}O_{19}$; $Ca_2MgSi_2O_7$) from calcium-aluminum inclusions (CAIs) in chondrites, cohenite ($(Fe,Ni)_3C$) in iron meteorites, and organic molecules and serpentines ($[Mg,Fe]_6Si_4O_{10}[OH]_8$) in carbonaceous chondrites. Other meteorite groups have distinctive elemental ratios in their silicate fraction, for example, calcium-rich pyroxene (fassaite) coupled with high-Ca plagioclase (anorthite) in angrites, and ordinary chondrites have very small ranges of Fe/Mg in silicates whereas the rare R chondrites exhibit a wide range of Fe/Mg ratios.

In this exercise, we consider a minimum scenario, which is how well classification based solely on the abundance of major phases (silicates, Fe-Ni metal, sulfides, phosphates, and oxides) and the Fe/Mg ratio (or Fe content) of the bulk silicate component could link microsamples shed from an asteroid to a unique meteorite class. We evaluated the number of particles that would need to be analyzed to accurately link the asteroid to a specific class of meteorites using a combination of a Monte Carlo method of generating sample sets and a multidimensional nearest-neighbor matching algorithm. We generated sample sets of n particles from the four mineral types (silicate, sulfides + phosphates, oxides, and Fe-Ni metal) by choosing random numbers from a uniform distribution [0,1] and assigning each number a particle type depending on its abundance in Table 1 (e.g., values between 0 and 0.692 would be labeled “silicate” in an enstatite chondrite that has an expected silicate particle abundance of 69.2%). We then compared the particle abundances to each meteorite class by calculating the probability that a sample from each class would create each random sample. The conditional probability of a specific abundance of particles of different types, $a_1, \ldots, a_n$, comprising a sample, s, given the sample matches a meteorite of class b, is calculated as

$$P(s \mid b) = (P(a_1 \mid b)^{s(a_1)} \cdot , \ldots, \cdot P(a_n \mid b)^{s(a_n)})^{-1} \quad (1)$$

where $P(a_1|b)$ is the probability of selecting particle of “type 1” once from the candidate class, and $s(a_1)$ is the number of “type 1” particles in the random sample.

We calculated the most likely meteorite class match to each simulated sample by evaluating the relative likelihoods of each candidate class yielding the sample. The relative likelihood of a class yielding a given sample is:

NASA Author Manuscript

NASA Author Manuscript

NASA Author Manuscript

$$LR_b = \frac{P(s \mid b)}{P(s \mid \neg b)} \quad (2)$$

where $P(s|\neg b)$ is the probability of the sample not being created from the candidate class b. Assuming that the random sample actually does belong to one of the meteorite types in Table 1, this probability is the sum of probabilities $P(s|b)$ calculated for all classes except the class in question. In other words, $\sum^{P}(s|\neg b_i)$ unity for all meteorite classes, b_1, …, b_n. The likelihood ratio, LR, is calculated for each class and the sample is assigned to the most likely class. The evidence strength of the selected class was evaluated using log-scale thresholds given by Jeffreys (1998) (Table 2). The basic assumption in evaluating the strength of the evidence that links a random sample to a meteorite class is that the confidence in the selection is proportional to the likelihood ratio corresponding to the selected class. As the likelihood ratio of the selected class increases, it provides stronger evidence that the sample truly belongs to the meteorite class.

We then constructed numerical test data sets derived from individual meteorite characteristics and applied this approach to see whether our method would correctly determine their class. We created numerical test data sets containing the published mineral abundance and silicate Fe/Mg ratio in Bluff (L5), Bath (H4), Abee (E), Juvinas (eucrite), and ALH A77801 and Dhofar 1222 (acapulcoites) (Table 3). Each test data set contained 1100 particles (chosen to match the Hayabusa sample set, discussed below) and each particle had an identity proportional to the abundance in Table 3. From each test data set, we conducted interval trials, where each trial selected n particles from the probability distribution to create a “sample” that we assumed to be the bulk composition of the meteorite. We then compared the bulk composition derived from the n particles in the test data set to the composition of the 14 meteorite classes in Table 1 to determine the best-fit class for each “sample.” We varied n from 10 to 1100 in intervals of 20 and conducted 300 unique trials at each interval n. This approach provides the ability to probe the confidence in a meteorite class assignment as a function of the number of particles in a sample data set.

The results are shown Fig. 4. For Bluff and Bath, only about 100 particles were needed for 90% of trials to determine they are in the ordinary chondrite class; the specific subclass (L and H, respectively) became apparent in samples sizes of about 200 particles. The Abee enstatite chondrite and Juvinas eucrite were easily classified even with a few tens of particles. The model also illustrates where the method of using only average compositions may fail; for example, both acapulcoites were misclassified but not consistently (L chondrite and enstatite chondrite). However, it should be reiterated that additional information (multispectral data, range of composition within silicate minerals, etc.) would be likely be available during a mission to help distinguish these (and other) meteorite classes.

We applied our approach to the Hayabusa sample data to investigate whether a similar approach would have been able to link Itokawa samples to a specific meteorite group, if they had been encountered in situ rather than returned to the Earth. One consistent database of 1087 monomineralic Hayabusa particles shows that 83% are silicates (olivine, pyroxene, and feldspar) and these silicates have an Fe/Mg ratio of 0.43 (Nakamura et al. 2011) (Table 1). We used these abundances to generate numerical test data sets and trials as above. The best-

NASA Author Manuscript NASA Author Manuscript NASA Author Manuscript

fit parent body for each trial using the Hayabusa data set is illustrated in Fig. 5. For trials of smaller numbers of particles (n<100), the samples may appear to derive from 7 of the 14 parent bodies considered, having some chance of being similar to basaltic achondrites, ordinary chondrites, carbonaceous, and enstatite chondrites. At around 100 particles, the sample is clearly distinguished (90% of all trials) as an ordinary chondrite, though multiple subtypes are still in play. When n reaches 200 particles, the sample is consistently closest to an LL-type ordinary chondrite (90% of all trials). However, only 60% of the n = 200 assignments are made with evidence that can be considered "substantial" or stronger. The evidence that the meteorite class is LL-type and not another class is "strong" or higher at n = 700. In trials with large numbers of particles, the second-choice class is the very similar L chondrites, where the occurrence of weakly evidenced selections is proportional to the occurrence of L-type selections. When the sample size reaches the actual number of Hayabusa-returned particles (1087), the selected class is LL-type chondrites with an LR of 1020, which is decisive evidence that the sample is derived from an LL-chondrite. In the returned Hayabusa samples, their origin as LL chondrites was unequivocally established using oxygen isotopes and trace element analyses (Nakamura et al. 2011).

The Stardust mission returned particulate samples from the coma of comet Wild 2. The elemental composition of the Stardust samples is in broad agreement with the analyses made by the dust analyzer aboard the Halley mission (Flynn et al. 2006). Most of the particles are weakly constructed mixtures of nanometer-scale grains with occasional much larger (>1 mm) ferromagnesian silicates, Fe-Ni sulfides, and Fe-Ni metal (Zolensky et al. 2006). Organic molecules are also found in many of the grains (Sandford et al. 2006). However, many more monomineralic fragments were created by the breakup of the cometary particles upon capture in the aerogel (Joswiak et al. 2012). The characteristics of these <10 μm monomineralic particles, when examined as a microsample set, do not appear to link Wild 2 to carbonaceous chondrites, as might be expected, given the similarity of IDPs to CI meteorites (Fig. 2). It may be that the Stardust data set is too small to yield reliable statistics (n = 95), or that the bulk composition of Comet Wild-2 is not well represented by the subset of monomineralic grains. However, the Stardust samples are linked to IDPs by methods available in the laboratory, including trace elements in olivine, amorphous silicates known as GEMS, and the morphologic presentation of pyroxene as platelets and whiskers (Brownlee et al. 2006).

DUST CLOUD GENERATION AROUND ASTEROIDS

Having shown that mass spectroscopy of grains can be used to link microsamples to meteorite groups, we now consider the number and density of particles shed from asteroid parent bodies available to make such analyses. With the exception of active asteroids, a key process for such shedding is meteoroid impacts, which eject material, both neutral and charged, that become part of the environment, either as bound or unbound particles, around all airless bodies (Szalay and Horányi 2016a). The tenuous dust cloud is maintained by the continual bombardment of the surfaces by fast, interplanetary micrometeoroids. Such ejecta clouds were detected and characterized in situ by the Galileo mission during flybys of the icy moons of Jupiter (Europa, Ganymede, and Callisto), and also around the Moon by the

NASA Author Manuscript NASA Author Manuscript NASA Author Manuscript

LADEE mission (Krüger et al. 1999, 2000; Krivov et al. 2003; Sremčević et al. 2003, 2005; Horanyi et al. 2015; Szalay and Horányi 2015b).

To model micrometeorite-derived ejecta clouds near asteroids, we build upon an existing model for the dust distribution around asteroids near 1 au (Szalay and Horányi 2016a). This model employs the same initial velocity distribution of ejecta particles as inferred from measurements by the Lunar Dust Experiment (LDEX) on LADEE and assumes that the same distribution holds at other airless bodies near 1 au. LDEX was not a mass analyzer, but rather a very sensitive impact ionization dust detector capable of individually detecting dust grains with radii a >300 nm (Horányi et al. 2014). Throughout its operation from orbit, LDEX discovered that the permanently present, asymmetric dust cloud at the Moon is sustained primarily by the helion (HE), apex (AP), and anti-helion (AH) sporadic meteoroid sources, with the AP being the strongest producer of ejecta (Szalay and Horányi 2015a). A minor contribution from the anti-apex (AA) source near dusk was also noted in subsequent analysis to account for the low but appreciable densities near dusk (Szalay and Horányi 2016c).

At the Moon, the vast majority of grains in the ejecta cloud are gravitationally bound (Horanyi et al. 2015). For the much smaller asteroids, essentially all grains are unbound; bound grains only make up a few percent of the ejecta cloud even for 100 km radius airless bodies (Szalay and Horányi 2016a). Hence, with the exception of Ceres and Vesta, we assume that all asteroids from 1 to 3 au have negligible gravity with respect to the dynamics of ejected grains. With this assumption in place, the dust density distribution in the ecliptic plane near a small airless body is

$$n(r,\phi,a,d) = n_w\left(\frac{R}{r}\right)a_\mu^{-2.7}\sum_s w_s(d)\cos^3(\phi-\phi_0)\Theta(\mid\phi-\phi_0\mid-\pi/2) \tag{3}$$

where $n_w = 5\times10^{-4}$ m^{-3}, R is the radius of the airless body, r is the distance from the center of the airless body, a_μ is the particle radius in μm, s is the index indicating the source (HE, AP, AH, or AA), w_s is the relative weight of the source that is a function of the heliocentric distance d, ϕ_s is the angle of the given source from apex, and Θ is the Heaviside function.

To extend this model to different heliocentric distances, we must make some additional assumptions about the sporadic sources. The HE/AH sources are generated by prograde short period Jupiter family comets (JFCs) (Nesvorny et al. 2011). The AP source is generated by particles on retrograde orbits shed from both Oort cloud comets (OCCs) and Halley-type comets (HTCs) (Wiegert et al. 2009; Nesvorny et al. 2011). While the retrograde OCC and HTC grains are significantly less numerous than JFCs at 1 au, the measured lunar dust cloud was found to be primarily caused by these particles as their impact velocities are so large. Quantitatively, the production of impact ejecta is given by

$$w_s = CF_{\mathrm{imp}}(d)m_{\mathrm{imp}}^{\alpha+1}(d)v_{\mathrm{imp}}^{\delta}(d) \tag{4}$$

where C is a fitting constant, F_{imp} is incident number flux, m_{imp} the characteristic mass, v_{imp} the incident velocity, and $\alpha = 0.2$ and $\delta = 2.5$ are fit constants from laboratory impact ejecta

NASA Author Manuscript NASA Author Manuscript NASA Author Manuscript

experiments (Koschny and Grün 2001; Krivov et al. 2003). At 1 au, $w_s(1) = [0.24, 0.49, 0.24, 0.03]$, building on previous analyses (Szalay and Horányi 2016a, 2016c).

To determine the production rate, $w_s(d)$, for heliocentric distance $d > 1$ au, we use Equation 4 and make four further assumptions: (1) impactor fluxes from the relative sources scale as given in Poppe (2016); (2) characteristic masses do not change as a function of d; and (3) that all asteroids are on circular Keplerian orbits and all impact velocities scale like $1 / \sqrt{d}$, following Kepler's law. For the flux scaling, we use the values given in Poppe (2016) for impactor fluxes onto a body in a circular orbit for various sources as a function of d for 100 μm grains. Since the OCC grain flux decreases faster than HTCs with distance from 1 to 3 au, we assume the AP source scales as HTCs. For the HE/AH sources, we use the scaling from the JFCs in this model. The assumption that the impactor velocities scale as $1 / \sqrt{d}$ is certainly reasonable for the AP source, as to first order this can be approximated as head-on collisions between circular retrograde grains and the circular prograde orbit of the airless body. The AA source is relatively unimportant in this scenario, scaling approximately following Kepler's law. For the HE/AH velocity scaling, without a complex particle tracing model to predict the change in impacting velocity distribution function, we also use Kepler's law to estimate a reasonable zeroth-order velocity scaling. With these assumptions and utilizing the values of $w_s(d = 1)$ as previously determined (Szalay and Horányi 2016a), we can then numerically calculate $w_s(d)$. A targeting study on eccentric asteroid 3200 Phaethon revealed that the eccentricity or the asteroid can modulate the expected ejecta production (Szalay et al. 2019a); however, we fix the orbits to be circular in this study to provide a baseline comparison. One last assumption relating to Equation 3 is that the relative angle from apex for the HE/AH sources remains the same from 1 to 3 au. While this angle would most likely also change to a certain extent as a function of d, without significant additional modeling to inform on this angle, we make the simplifying assumption that it remains constant.

Figure 6 shows that the calculated ejecta cloud density distribution for a 10-km radius airless body at 1 and 3 au, for grains with radii $a > 50$ nm. The lily pad structure of the ejecta cloud at 1 au is identical to previous work (Szalay and Horányi 2016a), and shown in a reference frame with the Sun in the $-x$ direction and apex (the direction of orbital motion) in the $+y$ direction. The impact rates at dusk remain poorly constrained; hence, the density of the ejecta cloud over this hemisphere remains only a qualitative estimate.

The most apparent and expected trend exhibited in Fig. 6 is the decrease in absolute number density as a function of heliocentric distance. Since both the fluxes and impact velocities decrease with heliocentric distance, the subsequent impact ejecta production also decreases following Equation 4. A secondary effect is the slight modification of the ejecta cloud structure due to changes in the relative importance of the various sources. Because the velocities are all forced to follow the same scaling and the relative angles remain the same, a consequence of the assumptions outlined above, the primary modification in structure arises from relative differences in flux between the AP and HE/AH sources. Since the HTC flux decreases more rapidly than the JFC flux, the AP source is diminished at 3 au on the right panel of Fig. 6. This flattened structure is a direct consequence of the model used and may vary for different cometary dust models. Overall, however, the structure is similar for ejecta

NASA Author Manuscript NASA Author Manuscript NASA Author Manuscript

clouds around asteroids from 1 to 3 au, namely that the density distribution is always enhanced on the apex side and the density will decrease for increased heliocentric distance.

In order to predict impact rates and the total number of particles a dust detector would encounter on a flyby mission to an asteroid, we first investigate the minimum dust size for a reliable detection and analysis. Assuming an LDEX type instrument with a similar sensitivity of 3000 electrons of impact plasma necessary to individually detect an impacting dust grain and an impact plasma dependence of $Q(\upsilon) \propto m\upsilon^{\beta}$, we calculate the minimum detectable size as a function of impact velocity. Due to the low impact velocities (about 1.6 km s^{-1}), the LDEX instrument was able to verify the power law character of the lunar ejecta dust distribution only for ≥300 nm-sized particles, with a cumulative particle size distribution index of −2.7. As an approximation, we assume that the size distribution function of ejecta particles from asteroids follows a similar law down to 50 nm. To calculate total impact numbers, we assume the effective detector area of 600 cm^2, which is the capability of recently developed dust analyzer instruments.

Figure 7 shows the minimum detectable particle size for four separate calibration curves. The original calibration of LDEX reported an impact velocity dependence of $\beta = 4.74$ (Horányi et al. 2014). More recent calibrations indicate that the exponent may be $\beta = 5.0$; therefore, we calculated the size dependence for both exponents. Additionally, we use two different mass density values, 2.5 and 3.33 g cc^{-1}, to represent a reasonable range for asteroidal ejecta particles. The subsequent four curves then represent an approximate bounding parameter space for the size dependence, which is similar for all curves. As an example, impact (or flyby) velocities of ~5 km s^{-1} would allow for individual detection of grains with $a \geq 50$ nm. We use a detection threshold of $a \geq 50$ nm for the following analyses.

With the size threshold in place, using Equation 3 and the analysis discussed in the previous section, we can determine the dust density distribution near an asteroid and flyby impact rates. Figure 8 shows an example flyby for a body of radius $R = 10$ km at heliocentric distance $d = 1.5$ au. The ejecta cloud density distribution is a hybrid of the 1 and 3 au cases (Fig. 6). The left panel shows the encountered number density along the flyby (at various altitudes, h, above the surface) as a function of distance from closest approach, as well as the total cumulative impacts. The solid lines denote apex-hemisphere flybys. Note, the values of h for each flyby are different from the impact parameter (measured from the center of the body) shown in a previous, similar analysis (Szalay and Horányi 2016a). The left panel shows the number density along the flyby as a function of distance from closest approach as well as the total cumulative impacts. Transits on the apex side (solid lines) result a factor of ~3 times larger number of total impacts for a given flyby altitude. As evidenced by the impact profile, the majority of the impacts occur within ±100 km from closest approach.

Similar analyses can then be repeated over a grid of heliocentric distance and flyby altitude for various asteroid sizes to determine the optimum parameters for a required number of collected dust impacts. Figure 9 shows the total number of expected dust impacts as a function of d and flyby altitude for detection particle size threshold $a \geq 50$ nm. The results can be scaled to a larger dust size threshold, $a > a_0$, using a $N(a) = N_0 (a/a_0)^{-2.7}$ where N_0 is the number of impacts given in Fig. 9 and $a_0 = 50$ nm. The largest impact rates would be

NASA Author Manuscript NASA Author Manuscript NASA Author Manuscript

measured for flybys near the surface, at smaller heliocentric distances, and near larger bodies. The specific dependencies of the total impact count on body radius, altitude, and heliocentric distance are a function of both the geometry of the flyby orbit and the relative strengths of the various dust sources.

It should be noted that this analysis represents only a lower limit to the dust density. There are additional sources of dust that could modify the size/number distribution of ejecta, many of which may have relatively low ejection velocities but could contribute to the overall number density. LDEX was only able to determine the dust density distribution down to altitudes of approximately 1 km, which corresponds to particles which left the surface with approximately 60 m s^{-1}. It is possible that the velocity distribution function has an enhancement at initial speeds lower than this. However, for the 50 nm grains discussed primarily in this work, radiation pressure (RP) can significantly alter trajectories within 1000 km of the body for initial speeds on the order of tens of m s^{-1}, which could effectively sweep out such grains from the measurement density distribution. Figure 10 shows an example of such a process. Here, we include only the force of RP, assuming the grains are spherical and perfectly reflecting and that the asteroid is at 1 au to represent the strongest case of RP. Dots show the location of particles launched from a uniform grid in angle from the surface of the airless body. As shown in this figure, particles with initial speeds on the order of 10 m s^{-1} or lower would experience a deviation from straight-line trajectories, modifying the dust density distribution.

DISCUSSION

Linking Particles to Parent Bodies

Despite the wide diversity of meteorites and the complexities of their compositions, major mineralogy and silicate Fe/Mg ratios are generally sufficient to distinguish major groups of meteorites from each other, given a sufficient number of particles. The number of particles needed to make a decisive determination of the meteorite group varies but is generally in the hundreds of grains. This analysis assumes that the elemental analysis of each microsample is both precise and accurate. The precision and accuracy of the individual analyses depend on many factors, including the particle speed, ionization potential, instrument calibration, etc. However, because we have simplified the analysis to basic mineralogy, the measurement precision of each analysis need only be sufficient to recognize it as a silicate, metal, oxide, or sulfide, which is well within the capabilities of current instrumentation. Our approach also assumes that each grain is monomineralic, and that information about individual minerals can be extracted from the mass spectrum. The micrometer-sized grains in the Hayabusa and Stardust collections were usually polymineralic, but the proportion of monomineralic grains and fragments increased with smaller grain sizes, increasing the chances that a dust grain measuring 50–100 nm would be monomineralic. Even these small particles, when encountered at flyby speeds, would yield adequate elemental analyses, as they consist of tens of millions of atoms. Grains measuring a few nm and larger were successfully analyzed using the Cassini CDA (Hsu et al. 2015).

Our simple approach using only a few minerals and element ratios highlights where potential confusion may arise, requiring additional information to help distinguish the

NASA Author Manuscript NASA Author Manuscript NASA Author Manuscript

classes. Several types of meteorites may be recognizable by the presence of unique minerals that would be identifiable using additional elemental lines and ratios, for example: oldhamite ([Ca,Mg]S) in enstatite chondrites, graphite (C) in ureilites, hibonite and mellilite ($CaAl_{12}O_{19}$; $Ca_2MgSi_2O_7$) from CAIs in chondrites, cohenite ($[Fe,Ni]_3C$) in iron meteorites, and organic molecules and serpentines ($[Mg,Fe]_6Si_4O_{10}[OH]_8$) in carbonaceous chondrites. Other meteorite groups have distinctive minerals that occur together in their silicate fraction, for example, calcium-rich pyroxene (fassaite) coupled with high-Ca plagioclase (anorthite) in angrites. The dispersion of compositions can also be a clue to meteorite origin, for example, the equilibrated ordinary chondrites have a very small range of Fe/Mg in silicates whereas the rare R chondrites exhibit a wide range of Fe/Mg ratios.

Important contextual measurements (e.g., imaging and multispectral/hyperspectral analysis) can constrain possible matches by narrowing the possible interpretation space. For example, pallasites and enstatite chondrites are similar to each other using only these parameters, whereas they would be easily distinguished in infrared spectroscopy. Take, for example, the NEAR mission, where global measurements of Fe, K, and Th indicate that the elemental composition of Eros' surface is consistent with that of chondrites (Peplowski 2016), but constraints from gamma ray and near-infrared spectroscopy rule out carbonaceous chondrites (McCoy et al. 2001), Ca/Si ratios rule out enstatite chondrites (Lim and Nittler 2009), and X-ray spectral data rule out H chondrites (Foley et al. 2006). Taken together, the data sets indicate that Eros' measured surface composition is best matched by the L and LL chondrites, which would provide strong constraints to interpretation of microsamples encountered around this asteroid. These measurements of the surface of Eros and other asteroids, along with the Cassini measurements of dust particles derived from interplanetary sources (Hillier et al. 2007), also illustrate that the surface materials of airless bodies are not hopelessly altered by billions of years of micrometeorite impacts. The surfaces of such bodies undergo space weathering, comminution, and likely contributions from impacting bodies, but their surfaces are recognizable in the context of meteorites (e.g., McSween et al. 2013); microsamples shed from these surfaces by spallation and electrostatic lofting would not be expected to have been rendered unrecognizable in the process.

Development of Dust Clouds Around Asteroids

Our modeling provides a lower limit to the amount of dust lofted from asteroids, modeling solely the contribution from micrometeorite impact. It is possible that other mechanisms may contribute appreciably to the number density, including surface grain size, jetting (as observed on Bennu), and electrostatically lofting. Recently visited asteroids, Bennu and Ryugu, have an overall larger grain size and more exposed hard surfaces than the Moon's regolith (Lauretta et al. 2019; Watanabe et al. 2019). Impact ejecta observations and comparison to impactor models suggest that the Moon's fine regolith surface may have a lower yield than an equivalent solid surface of the same material, where a larger fraction of impact energy may get partitioned to local heating of the regolith instead of into the kinetic energy of ballistic ejecta (Pokorný et al. 2019; Szalay et al. 2019b). Therefore, a harder asteroidal surface could produce significantly higher ejecta yields than the Moon's regolith surface, from which these predictions were derived. Additionally, asteroids with large eccentricity will experience enhanced ejecta production on their ram hemisphere (Szalay et

NASA Author Manuscript

NASA Author Manuscript

NASA Author Manuscript

al. 2019a) and a flyby near an eccentric asteroid near its ram hemisphere would boost total dust detections.

While LDEX searched for a population of small (100 nm) grains electrostatically lofted to high altitudes, it found no evidence of such a population within the detection limits (Szalay and Horányi 2015b). Additional remote sensing efforts at the Moon have also only yielded upper limits to the total population of high-altitude lofted dust (Glenar et al. 2011, 2014; Feldman et al. 2014). These observations do not preclude the possibility of small-scale electrostatic transport ejecting appreciable quantities of dust. Recent laboratory experiments indicate that a large degree of small-scale mobilization occurs for dusty surfaces exposed to relatively simple photo or plasma conditions (Wang et al. 2016). However, any process which ejects particles with speeds on the order of tens of m s^{-1} or less would be subjected to RP as discussed for the low velocity ejecta. Whether such processes could significantly augment the highly energetic impact ejecta process remains unclear.

Several key assumptions were introduced to simplify the mathematical and modeling complexity involved in created impact ejecta predictions. These assumptions may have appreciable effects that might need to be considered in future mission planning. One key assumption is that all encountered bodies are on circular, Keplerian orbits. This serves to simplify the ejecta cloud structure, as for bodies with circular orbits, we would expect that the ejecta cloud to be approximately symmetric about the apex direction. Additionally, it allows us to directly utilize the Poppe (2016) results for fluxes onto circular orbits. However, for bodies which have sufficiently large eccentricities, large seasonal variations would be expected as the relative velocity vector between the body and the sporadic sources varies throughout the year. Since the ejecta response function is highly velocity dependent, eccentric bodies would have asymmetric ejecta distributions. Were a spacecraft to encounter an eccentric body, it would measure enhanced dust impact rates on the hemisphere of the body with the largest relative velocity to the HE/AH source. A prime example of this phenomena occurs at Mercury, whose large eccentricity causes highly asymmetric distributions in impact vaporization (Pokorný et al. 2017). Additionally, the relative angles of the HE/AH sources will also vary with both eccentricity and heliocentric distance.

For the nominal flybys considered, we calculated predicted impact rates for transits in the ecliptic plane. Were a flyby to transit with a nonecliptic geometry, the nonequatorial sporadic sources would need to be included into the model, namely, the northern and southern toroidal sources which are understood to be generated by highly inclined HTCs (Pokorný et al. 2014). While the toroidal sources are significantly lower in flux, their large impact velocities may result in these sources playing a large role in generating impact ejecta in mid and especially high latitudes, similar to how the AP source is the dominant ejecta producer at the Moon due to its large velocity. Even in the ecliptic plane, the relative contributions of the retrograde HTCs and OCCs generating the AP source to the JFCs generating the HE/AH sources remain relatively unconstrained past 1 au. Future modeling efforts could shed light on this issue and would improve estimates for impact ejecta distributions throughout the solar system.

NASA Author Manuscript NASA Author Manuscript NASA Author Manuscript

Last, there is always the possibility, while small, that a given flyby occurs during a meteoroid shower at the target asteroid. During the LADEE mission, LDEX recorded significant enhancements due to meteoroid stream activity, most notably during the Geminids which caused an increase of tenfold in the number of dense ejecta plumes detected compared to the sporadic background (Szalay and Horányi 2016b; Szalay et al. 2018). The meteoroid environment, specifically the meteoroid streams, is particularly unconstrained outside of 1 au. Yet, if the environment past 1 au is similar to Earth's in meteoroid activity, asteroids could experience a handful of intense meteoroid streams each of which lasts few days that could liberate significantly larger quantities of impact ejecta than the nominal sporadic sources.

Instrument Improvements

Even with modest performance (mass resolution of $m/\Delta m$ ~30–100), dust detector-mass analyzer instruments have contributed major scientific discoveries, as discussed above. Over the past decade, much more capable in situ dust analyzer instruments have been developed (Srama et al. 2006; Sternovsky et al. 2007, 2011). These instruments combine large effective detector areas (≥600 cm^2) with time-of-flight, reflectron-type impact mass spectrometers. The SUrface Dust Analyser (SUDA), selected to fly on board the Europa Clipper mission to measure the composition of ballistic dust particles populating the thin exospheres around the Galilean moons, has an effective mass resolution $m/\Delta m$ of 200–250 over mass 1–250 (Kempf et al. 2014). The Interstellar Dust Experiment, selected to fly on the Interstellar Mapping and Acceleration Probe (IMAP) mission, will provide the elemental composition, speed and mass distributions of interstellar dust particles, with an effective mass resolution $m/\Delta m$ of ~200 over mass 1–500 (McComas et al. 2018). Together with ongoing technologic development, continued laboratory testing and calibration are continuing to improve the analytical robustness and accuracy of in situ microsample analysis.

CONCLUSIONS

The major meteorite groups may be distinguished from one another using indicators such as mineral abundance and elemental ratios. Several hundreds of microsamples derived from the meteorite bulk composition, if randomly ejected and encountered, would readily accomplish the goal of linking mineral abundance and composition with known meteorite types. Our modeling shows that hundreds of samples shed from a parent body could be collected and analyzed at relevant speeds during flybys of individual asteroids, depending on the mission design, and that these numbers are sufficient to robustly link dust samples to known meteorite classes.

The abundance of microsamples around asteroids is a function of the parent body radius, heliocentric distance, and altitude above the surface. Encountering thousands of these particles shed from larger, Main Belt asteroids would be accomplishable with spacecraft that comes within a body radius of the surface. Hundreds of microsamples may still be measured from near-Earth asteroids or small Main Belt asteroids during a close encounter (either by the main spacecraft or secondary payloads, where the secondary could make a low pass and report data to the primary), or by increasing the effective area of the dust sampling

NASA Author Manuscript NASA Author Manuscript NASA Author Manuscript

instrument. If smaller numbers of microsamples were encountered, constraints on parent body types might still be usefully inferred by examining the dispersion of compositions, detecting diagnostic phases (e.g., hydrated silicates, carbonates, organic molecules, and silicate compositions unique to specific meteorite groups, such as oldhamite or fassaite), and combining microsample analysis with other remote methods of determining composition, such as spectroscopy.

Dust analyzer instrumentation is steadily advancing, taking advantage of technological advancements in electronics, materials, and mechanical designs. Future dust detector instruments may be expected to have large sensitive areas, low mass, and improved dynamical sensitivity for compositional analyses. The velocity of incoming particles provides additional constraints on the source of the detected particles (e.g., interplanetary versus interstellar). With a high-performance dust trajectory sensor, particle ballistic paths may be traced back to their point of origin (Postberg et al. 2011), relating the measured composition of the grain to parent-body geologic features. Ideal flyby speeds for such analyses would be between 3 and 7 km s^{-1} to retrieve both elemental and molecular composition of the particles, but even at speeds greater than ~15 km s^{-1}, full elemental analysis may be conducted.

Given the compositional diversity of asteroids, and their distribution in space, it is implausible to consider returning samples from each one to establish their origin. However, sample return to Earth is not the only method for asteroidal sample analysis. The impact ejecta clouds that are continually sustained around asteroids provide a rich and so far untapped resource, and can provide crucial insight into understanding the origin and evolution of airless bodies in the solar system. In situ dust analyzers may be enabling for future missions to obtain the elemental and mineralogical composition measurement of dust particles originating from airless bodies without returning the samples to terrestrial laboratories (Rivkin et al. 2016).

Acknowledgments

This work was supported by the Johns Hopkins University Applied Physics Laboratory and the NASA Solar System Exploration Virtual Institute (SSERVI)—in particular, B. Cohen received support through the CLASS (Center for Lunar and Asteroid Surface Science) node, and M. Horanyi and Z. Sternovsky acknowledge support through the IMPACT (Institute for Modeling Plasmas, Atmosphere and Cosmic Dust) node. A. Rivkin acknowledges support from the NASA Near Earth Objects Observation program grant NNX14AL60G. Thoughtful reviews by the Associate Editor and two anonymous reviewers strengthened this manuscript. We use the NASA Astrophysical Data System Abstract Service.

REFERENCES

Altobelli N, Grün E, and Landgraf M 2006 A new look into the Helios dust experiment data: Presence of interstellar dust inside the Earth's orbit. Astronomy & Astrophysics 448:243–252.

Altobelli N, Postberg F, Fiege K, Trieloff M, Kimura H, and Sterken VJ 2016 Flux and composition of interstellar dust at Saturn from Cassini's cosmic dust analyzer. Science 352:312–318. 10.1126/science.aac6397. [PubMed: 27081064]

Altwegg K, Balsiger H, Bar-Nun A, Berthelier J, Bieler A, Bochsler P, Briois C, Calmonte U, Combi M, De Keyser J, Eberhardt P, Fiethe B, Fuselier S, Gasc S, Gombosi T, Hansen KC, Hässig M, Jäckel A, Kopp E, Korth A, LeRoy L, Mall U, Marty B, Mousis O, Neefs E, Owen T, Rème H,

NASA Author Manuscript NASA Author Manuscript NASA Author Manuscript

Rubin M, Sémon T, Tzou CY, Waite H, and Wurz P 2014 67P/Churyumov-Gerasimenko, a Jupiter family comet with a high D/H ratio. Science 347:1261952. [PubMed: 25501976]

Binzel RP, Rivkin AS, Bus SJ, Sunshine JM, and Burbine TH 2001 MUSES-C target asteroid (25143) 1998 SF36: A reddened ordinary chondrite. Meteoritics & Planetary Science 36:1167–1172.

Bischoff A, Clayton R, Markl G, Mayeda T, Palme H, Schultz L, Srinivasan G, Weber H, Weckwerth G, and Wolf D 2000 Mineralogy, chemistry, noble gases, and oxygen-and magnesium-isotopic compositions of the angrite Sahara 99555. Meteoritics & Planetary Science 35:A27.

Bland PA, Cressey G, and Menzies ON 2004 Modal mineralogy of carbonaceous chondrites by X-ray diffraction and Mössbauer spectroscopy. Meteoritics and Planetary Science 39:3–16.

Bowman LE, Papike JJ, and Spilde MN 1996 Modal abundances in diogenites: Insights into phase percentages using electron microprobe techniques (abstract #147). 27th Lunar and Planetary Science Conference CD-ROM.

Brearley AJ 2006 The action of water In Meteorites and the early solar system II, edited by Lauretta DS and McSween HY Jr. Tucson, Arizona: University of Arizona pp. 1:584–624.

Brownlee DE 1985 Cosmic dust: Collection and research. Annual Review of Earth and Planetary Sciences 13:147–173.

Brownlee D, Tsou P, Aléon J, Alexander CMOD, Araki T, Bajt S, Baratta GA, Bastien R, Bland P, Bleuet P, Borg J, Bradley JP, Brearley A, Brenker F, Brennan S, Bridges JC, Browning ND, Brucato JR, Bullock E, Burchell MJ, Busemann H, Butterworth A, Chaussidon M, Cheuvront A, Chi M, Cintala MJ, Clark BC, Clemett SJ, Cody G, Colangeli L, Cooper G, Cordier P, Daghlian C, Dai Z, D'Hendecourt L, Djouadi Z, Dominguez G, Duxbury T, Dworkin JP, Ebel DS, Economou TE, Fakra S, Fairey SAJ, Fallon S, Ferrini G, Ferroir T, Fleckenstein H, Floss C, Flynn G, Franchi IA, Fries M, Gainsforth Z, Gallien J-P, Genge M, Gilles MK, Gillet P, Gilmour J, Glavin DP, Gounelle M, Grady MM, Graham GA, Grant PG, Green SF, Grossemy F, Grossman L, Grossman JN, Guan Y, Hagiya K, Harvey R, Heck P, Herzog GF, Hoppe P, Hörz F, Huth J, Hutcheon ID, Ignatyev K, Ishii H, Ito M, Jacob D, Jacobsen C, Jacobsen S, Jones S, Joswiak D, Jurewicz A, Kearsley AT, Keller LP, Khodja H, Kilcoyne ALD, Kissel J, Krot A, Langenhorst F, Lanzirotti A, Le L, Leshin LA, Leitner J, Lemelle L, Leroux H, Liu M-C, Luening K, Lyon I, MacPherson G, Marcus MA, Marhas K, Marty B, Matrajt G, McKeegan K, Meibom A, Mennella V, Messenger K Messenger S, Mikouchi T, Mostefaoui S, Nakamura T, Nakano T, Newville M, Nittler LR, Ohnishi I, Ohsumi K, Okudaira K, Papanastassiou DA, Palma R, Palumbo ME, Pepin RO, Perkins D, Perronnet M, Pianetta P, Rao W, Rietmeijer FJM, Robert F, Rost D, Rotundi A, Ryan R, Sandford SA, Schwandt CS, See TH, Schlutter D, Sheffield-Parker J, Simionovici A, Simon S, Sitnitsky I, Snead CJ, Spencer MK, Stadermann FJ, Steele A, Stephan T, Stroud R, Susini J Sutton SR, Suzuki Y, Taheri M, Taylor S, Teslich N, Tomeoka K, Tomioka N, Toppani A, Trigo-Rodríguez JM, Troadec D, Tsuchiyama A, Tuzzolino AJ, Tyliszczak T, Uesugi K, Velbel M, Vellenga J, Vicenzi E, Vincze L, Warren J, Weber I, Weisberg M, Westphal AJ, Wirick S, Wooden D, Wopenka B, Wozniakiewicz P, Wright I, Yabuta H, Yano H, Young ED, Zare RN, Zega T, Ziegler K, Zimmerman L, Zinner E, and Zolensky M 2006 Comet 81P/Wild 2 under a microscope. Science 314:1711–1716. [PubMed: 17170289]

Burbine TH and Binzel RP 2002 Small main-belt asteroid spectroscopic survey in the near-infrared. Icarus 159:468–499.

Bus SJ and Binzel RP 2002 Phase II of the small main-belt asteroid spectroscopic survey: A feature-based taxonomy. Icarus 158:146–177.

Buseck PR 1977 Pallasite meteorites—Mineralogy, petrology and geochemistry. Geochimica et Cosmochimica Acta 41:711–721.

Campins H, Hargrove K, Pinilla-Alonso N, Howell ES, Kelley MS, Licandro J, Mothé-Diniz T, Fernandez Y, and Ziffer J 2010 Water ice and organics on the surface of the asteroid 24 Themis. Nature 464:1320–1321. [PubMed: 20428164]

Dikov YP, Evlanov EN, Fomenkova MN, Mukhin LM, Nazarov MA, Prilutsky OF, Sagdeev RZ, and Zubkov BV 1989 Halley comet dust particle classification according to the data obtained by mass spectrometer Puma-2. Advances in Space Research 9:253–258. [PubMed: 11537300]

Feldman PD, Glenar DA, Stubbs TJ, Retherford KD, Gladstone GR, and Miles PF 2014 Upper limits for a lunar dust exosphere from far-ultraviolet spectroscopy by LRO/LAMP. Icarus 1–34. [PubMed: 24817768]

NASA Author Manuscript NASA Author Manuscript NASA Author Manuscript

Fiege K, Trieloff M, Hillier JK, Guglielmino M, Postberg F, and Srama R 2014 Calibration of relative sensitivity factors for impact ionization detectors with high-velocity silicate microparticles. Icarus 241:336–345.

Flynn GJ, Bleuet P, Borg J, Bradley JP, Brenker FE, Brennan S, Bridges J, Brownlee DE, Bullock ES, Burghammer M, Clark BC, Dai ZR, Daghlian CP, Djouadi Z, Fakra S, Ferroir T, Floss C, Franchi IA, Gainsforth Z, Gallien J-P, Gillet P, Grant PG, Graham GA, Green SF, Grossemy F, Heck PR, Herzog GF, Hoppe P, Hörz F, Huth J, Ignatyev K, Ishii HA, Janssens K, Joswiak D, Kearsley AT, Khodja H, Lanzirotti A, Leitner J, Lemelle L, Leroux H, Luening K, MacPherson GJ, Marhas KK, Marcus MA, Matrajt G, Nakamura T, Nakamura-Messenger K, Nakano T, Newville M, Papanastassiou DA, Pianetta P, Rao W, Riekel C, Rietmeijer FJM, Rost D, Schwandt CS, See TH, Sheffield-Parker J, Simionovici A, Sitnitsky I, Snead CJ, Stadermann FJ, Stephan T, Stroud RM, Susini J, Suzuki Y, Sutton SR, Taylor S, Teslich N, Troadec D, Tsou P, Tsuchiyama A, Uesugi K, Vekemans B, Vicenzi EP, Vincze L, Westphal AJ, Wozniakiewicz P, Zinner E, and Zolensky ME 2006 Elemental compositions of Comet 81P/Wild 2 samples collected by Stardust. Science 314:1731–1735. [PubMed: 17170294]

Foley CN, Nittler L, McCoy TJ, Lim L, Brown M, Starr RD, and Trombka JI 2006 Minor element evidence that Asteroid 433 Eros is a space-weathered ordinary chondrite parent body. 184, 338–343.

Fomenkova MN, Kerridge JF, Marti K, and McFadden LA 1992 Compositional trends in rock-forming elements of comet Halley dust. Science 258:266. [PubMed: 11538058]

Fujiwara A, Kawaguchi J, Yeomans D, Abe M, Mukai T, Okada T, Saito J, Yano H, Yoshikawa M, and Scheeres D 2006 The rubble-pile asteroid Itokawa as observed by Hayabusa. Science 312:1330–1334. [PubMed: 16741107]

Glenar DA, Stubbs TJ, McCoy JE, and Vondrak RR 2011 A reanalysis of the Apollo light scattering observations, and implications for lunar exospheric dust. Planetary and Space Science 59:1695–1707.

Glenar DA, Stubbs TJ, Hahn JM, and Wang Y 2014 Search for a high-altitude lunar dust exosphere using Clementine navigational star tracker measurements. Journal of Geophysical Research Planets 119:2548–2567.

Goldsworthy BJ, Burchell MJ, Cole MJ, Armes SP, Khan MA, Lascelles SF, Green SF, McDonnell JAM, Srama R, and Bigger SW 2003 Time of flight mass spectra of ions in plasmas produced by hypervelocity impacts of organic and mineralogical microparticles on a cosmic dust analyser. Astronomy & Astrophysics 409:1151–1167.

Grün E, Pailer N, Fechtig H, and Kissel J 1980 Orbital and physical characteristics of micrometeoroids in the inner solar system as observed by Helios 1. Planetary and Space Science 28:333–349.

Hillier J, Green S, McBride N, Altobelli N, Postberg F, Kempf S, Schwanethal J, Srama R, McDonnell J, and Grun E 2007 Interplanetary dust detected by the Cassini CDA Chemical Analyser. Icarus 190:643–654.

Hillier JK, Sternovsky Z, Armes SP, Fielding LA, Postberg F, and Bugiel S 2014 Impact ionisation mass spectrometry of polypyrrole-coated pyrrhotite microparticles. Planetary and Space Science 97:9–22. 10.1016/j.pss.2014.04.008.

Hillier JK, Sternovsky Z, Kempf S, Trieloff M, Guglielmino M, Postberg F, and Price MC 2018 Impact ionisation mass spectrometry of platinum-coated olivine and magnesite-dominated cosmic dust analogues. Planetary and Space Science 156:96–110. 10.1016/j.pss.2017.10.002.

Horányi M, Sternovsky Z, Lankton M, Dumont C, Gagnard S, Gathright D, Grün E, Hansen D, James D, Kempf S, Lamprecht B, Srama R, Szalay JR, and Wright G 2014 The Lunar Dust Experiment (LDEX) onboard the Lunar Atmosphere and Dust Environment Explorer (LADEE) mission. Space Science Reviews 185:93–113.

Horanyi M, Szalay J, Kempf S, Schmidt J, Grün E, Srama R, and Sternovsky Z 2015 A permanent, asymmetric dust cloud around the Moon. Nature 522:324–326. [PubMed: 26085272]

Hsu H-W, Postberg F, Sekine Y, Shibuya T, Kempf S, and Horányi M 2015 Ongoing hydrothermal activities within Enceladus. Nature 519:207–210. [PubMed: 25762281]

Jambon A, Barrat J-A, Boudouma O, Fonteilles M, Badia D, Göpel C, and Bohn M 2005 Mineralogy and petrology of the angrite Northwest Africa 1296. Meteoritics & Planetary Science 40:361–375.

NASA Author Manuscript NASA Author Manuscript NASA Author Manuscript

JAXA. 2016 Asteroid explorer “Hayabusa2.” http://global.jaxa.jp/projects/sat/hayabusa2/. Accessed December 12, 2016.

Jeffreys H 1998 The theory of probability. Oxford, UK: Oxford University Press.

Jessberger EK. Altwegg K. Ehrenfreund P. Geiss J. Huebner W. On the elemental, isotopic and mineralogical ingredients of rocky cometary particulates; Proceedings of the origin and composition of cometary materials; Dordrecht, the Netherlands. Kluwer Academic Publishers, Space Science Series of ISSI; 1999.

Joswiak DJ, Brownlee DE, Matrajt G, Westphal AJ, Snead CJ, and Gainsforth Z 2012 Comprehensive examination of large mineral and rock fragments in Stardust tracks: Mineralogy, analogous extraterrestrial materials, and source regions. Meteoritics & Planetary Science 47:471–524.

Kallemeyn GW, Rubin AE, and Wasson JT 1996 The compositional classification of chondrites: VII. The R chondrite group. Geochimica et Cosmochimica Acta 60:2243–2256.

Keil K 1962 Quantitativ-erzmikroskopische Integrationsanalyse der Chondrite. Chemie der Erde 22:281–348.

Keil K 1968 Mineralogical and chemical relationships among enstatite chondrites. Journal of Geophysical Research 73:6945–6976.

Keil K 2012 Angrites, a small but diverse suite of ancient, silica-undersaturated volcanic-plutonic mafic meteorites, and the history of their parent asteroid. Chemie der Erde 72:191–218.

Kempf S 2009 Dust spectroscopy of Jovian satellite surface composition. European Planetary Science Congress 2009:472.

Kempf S, Srama R, Grün E, Mocker A, Postberg F, Hillier JK, Horányi M, Sternovsky Z, Abel B, Beinsen A, Thissen R, Schmidt J, Spahn F, and Altobelli N 2012 Linear high resolution dust mass spectrometer for a mission to the Galilean satellites. Planetary and Space Science 65:10–20.

Kempf S, Altobelli N, Briois C, Grün E, Horanyi M, Postberg F, Schmidt J, Srama R, Sternovsky Z, and Tobie G 2014 SUDA: A dust mass spectrometer for compositional surface mapping for a mission to Europa. In European Planetary Science Congress, pp. EPSC2014–229.

Kissel JI 1986 The Giotto particulate impact analyser. ESA Special Publication ESA SP-1077:67–83.

Kissel J and Krueger F 1987 The organic component in dust from comet Halley as measured by the PUMA mass spectrometer on board Vega 1. Nature 326:755.

Kissel J, Brownlee DE, Büchler K, Clark BC, Fechtig H, Grün E, Hornung K, Igenbergs EB, Jessberger EK, and Krueger FR 1986 Composition of comet Halley dust particles from Giotto observations. Nature 321:336.

Kissel J, Glasmachers A, Grün E, Henkel H, Höfner H, Haerendel G, Von Hoerner H, Hornung K, Jessberger EK, and Krueger FR 2003 Cometary and interstellar dust analyzer for comet Wild 2. Journal of Geophysical Research: Planets 108.

Kissel J, Krueger FR, Silén J, and Clark BC 2004 The cometary and interstellar dust analyzer at comet 81P/Wild 2. Science 304:1774–1776. [PubMed: 15205526]

Koschny D and Grün E 2001 Impacts into ice-silicate mixtures: crater morphologies, volumes, depth-to-diameter ratios, and yield. Icarus 154:391–401.

Krivov AV, Sremčević M, Spahn F, Dikarev VV, and Kholshevnikov KV 2003 Impact-generated dust clouds around planetary satellites: Spherically symmetric case. Planetary and Space Science 51:251–269.

Krüger H, Krivov AA, Hamilton DP, and Grün E 1999 Detection of an impact-generated dust cloud around Ganymede. Nature 399:558–560.

Krüger H, Krivov AV, and Grün E 2000 A dust cloud of Ganymede maintained by hypervelocity impacts of interplanetary micrometeoroids. Planetary and Space Science 48:1457–1471.

Krüger H, Krivov AV, Sremčević M, and Grün E 2003 Impact-generated dust clouds surrounding the Galilean moons. Icarus 164:170–187.

Lauretta DS, Bartels AE, Barucci MA, Bierhaus EB, Binzel RP, Bottke WF, Campins H, Chesley SR, Clark BC, Clark BE, Cloutis EA, Connolly HC, Crombie MK, Delbó M, Dworkin JP, Emery JP, Glavin DP, Hamilton VE, Hergenrother CW, Johnson CL, Keller LP, Michel P, Nolan MC, Sandford SA, Scheeres DJ, Simon AA, Sutter BM, Vokrouhlický D, and Walsh KJ 2015 The OSIRIS-REx target asteroid (101955) Bennu: Constraints on its physical, geological, and dynamical nature from astronomical observations. Meteoritics & Planetary Science 50:834–849.

NASA Author Manuscript NASA Author Manuscript NASA Author Manuscript

Lauretta DS, DellaGiustina DN, Bennett CA, Golish DR, Becker KJ, Balram-Knutson SS, Barnouin OS, Becker TL, Bottke WF, and Boynton WV 2019 The unexpected surface of asteroid (101955) Bennu. Nature 568:55–60. [PubMed: 30890786]

Lim LF and Nittler LR 2009 Elemental composition of 433 Eros: New calibration of the NEAR-Shoemaker XRS data. Icarus 200:129–146.

Mann I and Jessberger EK 2010 The in-situ study of solid particles in the solar system In Astromineralogy, edited by Henning T Berlin: Springer pp. 233–257.

Mayne RG, McSween HY, McCoy TJ, and Gale A 2009 Petrology of the unbrecciated eucrites. Geochimica et Cosmochimica Acta 73:794–819.

McAdam MM, Sunshine JM, Howard KT, and McCoy TM 2015 Aqueous alteration on asteroids: Linking the mineralogy and spectroscopy of CM and CI chondrites. Icarus 245:320–332.

McComas DJ, Christian ER, Schwadron NA, Fox N, Westlake J, Allegrini F, Baker DN, Biesecker D, Bzowski M, and Clark G 2018 Interstellar mapping and acceleration probe (IMAP): A new NASA mission. Space Science Reviews 214:116.

McCoy TJ, Burbine TH, McFadden LA, Starr RD, Gaffey MJ, Nittler LR, Evans LG, Izenberg N, Lucey PG, Trombka JI, Bell Iii JF, Clark BE, Clark PE, Squyres SW, Chapman CR, Boynton WV, and Veverka J 2001 The composition of 433 Eros: A mineralogical—Chemical synthesis. Meteoritics & Planetary Science 36:1661–1672.

McSween HY, Binzel RP, De Sanctis MC, Ammannito D, Prettyman TH, Beck AW, Reddy V, Le Corre L, Gaffey MJ, McCord TB, and Raymond CA 2013 Dawn: The Vesta–HED connection; and the geologic context for eucrites, diogenites, and howardites. Meteoritics & Planetary Science 48:2090–2104.

Mittlefehldt DW, McCoy TJ, Goodrich CA, and Kracher A 1998 Non-chondritic meteorites from asteroidal bodies In Planetary materials, edited by Papike JJ, pp. 4-1–4-195. Washington, DC: Mineralogical Society of America.

Morbidelli A, Chambers J, Lunine JI, Petit JM, Robert F, Valsecchi GB, and Cyr KE 2000 Source regions and time scales for the delivery of water to Earth. Meteoritics & Planetary Science 35:1309–1320.

Nakamura T, Noguchi T, Tanaka M, Zolensky ME, Kimura M, Tsuchiyama A, Nakato A, Ogami T, Ishida H, Uesugi M, Yada T, Shirai K, Fujimura A, Okazaki R, Sandford SA, Ishibashi Y, Abe M, Okada T, Ueno M, Mukai T, Yoshikawa M, and Kawaguchi J 2011 Itokawa dust particles: A direct link between S-type asteroids and ordinary chondrites. Science 333:1113–1116. [PubMed: 21868667]

Nakamura E, Makishima A, Moriguti T, Kobayashi K, Tanaka R, Kunihiro T, Tsujimori T, Sakaguchi C, Kitagawa H, Ota T, Yachi Y, Yada T, Abe M, Fujimura A, Ueno M, Mukai T, Yoshikawa M, and Kawaguchi J 2012 Space environment of an asteroid preserved on micrograins returned by the Hayabusa spacecraft. Proceedings of the National Academy of Sciences of the USA 109:E624–E629. [PubMed: 22371561]

Nesvorny D, Vokrouhlický D, Pokorný P, and Janches D 2011 Dynamics of dust particles released from Oort cloud comets and their contribution to radar meteors. The Astrophysical Journal 743:1.

Peplowski PN 2016 The global elemental composition of 433 Eros: First results from the NEAR gamma-ray spectrometer orbital dataset. Planetary and Space Science 134:36–51.

Pizzarello S, Cooper G, and Flynn G 2006 The nature and distribution of the organic material in carbonaceous chondrites and interplanetary dust particles In Meteorites and the early solar system II, edited by Lauretta DS and McSween HY Jr. Tucson, Arizona: University of Arizona pp. 625–651.

Pokorný P, Vokrouhlický D, Nesvorný D, Campbell-Brown M, and Brown P 2014 Dynamical model for the toroidal sporadic meteors. The Astrophysical Journal 789.

Pokorný P, Sarantos M, and Janches D 2017 Reconciling the dawn–dusk asymmetry in mercury's exosphere with the micrometeoroid impact directionality. The Astrophysical Journal Letters 842:L17.

Pokorný P, Janches D, Sarantos M, Szalay JR, Horányi M, Nesvorný D, and Kuchner MJ 2019 Meteoroids at the Moon: Orbital properties, surface vaporization, and impact ejecta production. Journal of Geophysical Research: Planets 124:752–778.

NASA Author Manuscript NASA Author Manuscript NASA Author Manuscript

Poppe AR 2016 An improved model for interplanetary dust fluxes in the outer solar system. Icarus 264:369–386.

Postberg F, Kempf S, Schmidt J, Brilliantov N, Beinsen A, Abel B, Buck U, and Srama R 2009 Sodium salts in E-ring ice grains from an ocean below the surface of Enceladus. Nature 459:1098–1101. [PubMed: 19553992]

Postberg F, Grün E, Horanyi M, Kempf S, Krüger H, Schmidt J, Spahn F, Srama R, Sternovsky Z, and Trieloff M 2011 Compositional mapping of planetary moons by mass spectrometry of dust ejecta. Planetary and Space Science 59:1815–1825.

Postberg F, Fiege K, Altobelli N, Srama R, and Trieloff M 2014 Mass spectrometry of contemporary interstellar dust by the Cassini space craft. LPI Contributions 1800:5272.

Postberg F, Khawaja N, Abel B, Choblet G, Glein CR, Gudipati MS, Henderson BL, Hsu H-W, Kempf S, Klenner F, Moragas-Klostermeyer G, Magee B, Nölle L, Perry M, Reviol R, Schmidt J, Srama R, Stolz F, Tobie G, Trieloff M, and Waite JH 2018 Macromolecular organic compounds from the depths of Enceladus. Nature 558:564–568. 10.1038/s41586-018-0246-4. [PubMed: 29950623]

Reddy V, Li J-Y, Le Corre L, Scully JEC, Gaskell R, Russell CT, Park RS, Nathues A, Raymond C, Gaffey MJ, Sierks H, Becker KJ, and McFadden LA 2013 Comparing dawn, hubble space telescope, and ground-based interpretations of (4) Vesta. Icarus 226:1103–1114.

Reddy V, Dunn T, Thomas CA, Moskovitz N, and Burbine T 2015 Mineralogy and surface composition of asteroids In Asteroids IV. edited by Michel P, DeMeo FD, and Bottke WF Tucson, Arizona: University of Arizona Press.

Rivkin AS and Emery JP 2010 Detection of ice and organics on an asteroidal surface. Nature 464:1322–1323. [PubMed: 20428165]

Rivkin AS, Howell ES, Vilas F, and Lebovsky LA 2002 Hydrated minerals on asteroids: The astronomical record In Asteroids III, edited by Bottke WF, Cellino A, Paolicci P, and Binzel RP Tucson, Arizona: University of Arizona Press pp. 235–253.

Rivkin AS, Howell ES, Vervack RJ Jr, Magri C, Nolan MC, Fernandez YR, Cheng AF, Antonietta Barucci M, and Michel P 2013 The NEO (175706) 1996 FG3 in the 2-4 μm spectral region: Evidence for an aqueously altered surface. Icarus 223:493–498.

Rivkin AS, Anderson R, Barnouin O, Chabot N, Ernst C, Klima R, Leary J, Mehr L, Seifert H, Cohen BA, and Sternovsky Z 2016 The main-belt asteroid and NEO tour with imaging and spectroscopy (MANTIS). IEEE Aerospace Conference.

Rubin AE 1997 Mineralogy of meteorite groups. Meteoritics & Planetary Science 32:231–247.

Rubin AE 2007 Petrogenesis of acapulcoites and lodranites: A shock-melting model. Geochimica et Cosmochimica Acta 71:2383–2401.

Sandford SA, Aléon J, Alexander CMOD, Araki T, Bajt SA, Baratta GA, Borg J, Bradley JP, Brownlee DE, Brucato JR, Burchell MJ, Busemann H, Butterworth A, Clemett SJ, Cody G, Colangeli L, Cooper G, Hendecourt L, Djouadi Z, Dworkin JP, Ferrini G, Fleckenstein H, Flynn GJ, Franchi IA, Fries M, Gilles MK, Glavin DP, Gounelle M, Grossemy F, Jacobsen C, Keller LP, Kilcoyne ALD, Leitner J, Matrajt G, Meibom A, Mennella V, Mostefaoui S, Nittler LR, Palumbo ME, Papanastassiou DA, Robert F, Rotundi A, Snead CJ, Spencer MK, Stadermann FJ, Steele A, Stephan T, Tsou P, Tyliszczak T, Westphal AJ, Wirick S, Wopenka B, Yabuta H, Zare RN, and Zolensky ME 2006 Organics captured from Comet 81P/Wild 2 by the Stardust spacecraft. Science 314:1720–1724. [PubMed: 17170291]

Sekanina Z, Hanner MS, Jessberger EK, and Fomenkova MN 2001 Cometary dust In Interplanetary dust, edited by Grün E, Gustafson BAS, Dermott S, and Fechtig H Heidelberg: Springer pp. 95–161.

Singletary SJ and Grove TL 2003 Early petrologic processes on the ureilite parent body. Meteoritics & Planetary Science 38:95–108.

Spahn F, Schmidt J, Albers N, Hörning M, Makuch M, Seiß M, Kempf S, Srama R, Dikarev V, Helfert S, Moragas-Klostermeyer G, Krivov AV, Sremčević M, Tuzzolino AJ, Economou T, and Grün E 2006 Cassini dust measurements at Enceladus and implications for the origin of the E ring. Science 311:1416–1418. [PubMed: 16527969]

Srama R, Ahrens TJ, Altobelli N, Auer S, Bradley JG, Burton M, Dikarev VV, Economou T, Fechtig H, Görlich M, Grande M, Graps A, Grün E, Havnes O, Helfert S, Horanyi M, Igenbergs E,

NASA Author Manuscript NASA Author Manuscript NASA Author Manuscript

Jessberger EK, Johnson TV, Kempf S, Krivov AV, Krüger H, Mocker-Ahlreep A, Moragas-Klostermeyer G, Lamy P, Landgraf M, Linkert D, Linkert G, Lura F, McDonnell JAM, Möhlmann D, Morfill GE, Müller M, Roy M, Schäfer G, Schlotzhauer G, Schwehm GH, Spahn D, Stübig M, Svestka J, Tschernjawski V, Tuzzolino AJ, Wäsch R, and Zook HA 2004 The Cassini cosmic dust analyzer. Space Science Reviews 114:465–518.

Srama R, Srowig A, Rachev M, Grün E, Kempf S, Moragas-Klostermeyer G, Conlon T, Harris D, Auer S, Glasmachers A, Helfert S, Linnemann H, and Tschernjawski V 2006 Development of an advanced dust telescope. Earth Moon and Planets 95:211–220.

Sremčević M, Krivov AV, and Spahn F 2003 Impact-generated dust clouds around planetary satellites: Asymmetry effects. Planetary and Space Science 51:455–471.

Sremčević M, Krivov AV, Krüger H, and Spahn F 2005 Impact-generated dust clouds around planetary satellites: Model versus Galileo data. Planetary and Space Science 53:625–641.

Sternovsky Z, Amyx K, Bano G, Landgraf M, Horanyi M, Knappmiller S, Robertson S, Grün E, Srama R, and Auer S 2007 Large area mass analyzer instrument for the chemical analysis of interstellar dust particles. Review of Scientific Instruments 78:014501. [PubMed: 17503935]

Sternovsky Z, Grün E, Drake K, Xie J, Horányi M, and Srama R 2011 Novel instrument for dust astronomy: Dust telescope. IEEE Aerospace Conference #1–8.

Szalay JR and Horányi M 2015a Annual variation and synodic modulation of the sporadic meteoroid flux to the Moon. Geophysical Research Letters 42:10,580–10,584.

Szalay JR and Horányi M 2015b The search for electrostatically lofted grains above the Moon with the Lunar Dust Experiment. Geophysical Research Letters 42:5141–5146.

Szalay J and Horányi M 2016a The impact ejecta environment of near earth asteroids. The Astrophysical Journal Letters 830

Szalay JR and Horányi M 2016b Detecting meteoroid streams with an in-situ dust detector above an airless body. Icarus 275:221–231.

Szalay JR and Horányi M 2016c Lunar meteoritic gardening rate derived from in situ LADEE/LDEX measurements. Geophysical Research Letters 43:4893–4898.

Szalay JR, Pokorný P, Jenniskens P, and Horányi M 2018 Activity of the 2013 Geminid meteoroid stream at the Moon. Monthly Notices of the Royal Astronomical Society 474:4225–4231. 10.1093/mnras/stx3007. [PubMed: 29545651]

Szalay JR, Pokorný P, Horáanyi M, Janches D, Sarantos M, and Srama R 2019a Impact ejecta environment of an eccentric asteroid: 3200 Phaethon. Planetary and Space Science 165:194–204.

Szalay JR, Pokorny P, Sternovsky Z, Kupihar Z, Poppe AR, and Horányi M 2019b Impact ejecta and gardening in the lunar polar regions. Journal of Geophysical Research: Planets 124 10.1029/2018JE005756.

Takir D, Emery JP, McSween HY, Hibbitts CA, Clark RN, Pearson N, and Wang A 2013 Nature and degree of aqueous alteration in CM and CI carbonaceous chondrites. Meteoritics & Planetary Science 48:1618–1637.

Veverka J, Robinson M, Thomas P, Murchie S, Bell JF, Izenberg N, Chapman C, Harch A, Bell M, Carcich B, Cheng A, Clark B, Domingue D, Dunham D, Farquhar R, Gaffey MJ, Hawkins E, Joseph J, Kirk R, Li H, Lucey P, Malin M, Martin P, McFadden L, Merline WJ, Miller JK, Owen WM, Peterson C, Prockter L, Warren J, Wellnitz D, Williams BG, and Yeomans DK2000 NEAR at Eros: Imaging and spectral results. Science 289:2088–2097. [PubMed: 11000105]

Volquardsen EL, Rivkin AS, and Bus SJ 2007 Composition of hydrated near-Earth object (100085) 1992 UY4. Icarus 187:464–468.

Wang X, Schwan J, Hsu HW, Grün E, and Horányi M 2016 Dust charging and transport on airless planetary bodies. Geophysical Research Letters 43:6103–6110.

Watanabe S, Hirabayashi M, Hirata N, Noguchi R, Shimaki Y, Ikeda H, Tatsumi E, Yoshikawa M, Kikuchi S, and Yabuta H 2019 Hayabusa2 arrives at the carbonaceous asteroid 162173 Ryugu—A spinning top–shaped rubble pile. Science 364:268–272. 10.1126/science.aav8032 [PubMed: 30890588]

Weisberg MK, McCoy TJ, Krot AN, and McSween HY 2006 Systematics and evaluation of meteorite classification In Meteorites and the early solar system II, edited by Lauretta DS and McSween HY Jr. Tucson, Arizona: University of Arizona Press pp. 19–52.

NASA Author Manuscript

NASA Author Manuscript

NASA Author Manuscript

Wiegert PA, Vaubaillon J, and Campbell-Brown M 2009 A dynamical model of the sporadic meteoroid complex. Icarus 201:295–310.

Xu S, Binzel RP, Burbine TH, and Bus SJ 1995 Small main-belt asteroid spectroscopic survey: Initial results. Icarus 115:1–35.

Zolensky ME, Zega TJ, Yano H, Wirick S, Westphal AJ, Weisberg MK, Weber I, Warren JL, Velbel MA, Tsuchiyama A, Tsou P, Toppani A, Tomioka N, Tomeoka K, Teslich N, Taheri M, Susini J, Stroud R, Stephan T, Stadermann FJ, Snead CJ, Simon SB, Simionovici A, See TH, Robert F, Rietmeijer FJM, Rao W, Perronnet MC, Papanastassiou DA, Okudaira K, Ohsumi K, Ohnishi I, Nakamura-Messenger K, Nakamura T, Mostefaoui S, Mikouchi T, Meibom A, Matrajt G, Marcus MA, Leroux H, Lemelle L, Le L, Lanzirotti A, Langenhorst F, Krot AN, Keller LP, Kearsley AT, Joswiak D, Jacob D, Ishii H, Harvey R, Hagiya K, Grossman L, Grossman JN, Graham GA, Gounelle M, Gillet P, Genge MJ, Flynn G, Ferroir T, Fallon S, Ebel DS, Dai ZR, Cordier P, Clark B, Chi M, Butterworth AL, Brownlee DE, Bridges JC, Brennan S, Brearley A, Bradley JP, Bleuet P, Bland PA, and Bastien R 2006 Mineralogy and petrology of comet 81P/Wild 2 nucleus samples. Science 314:1735–1739. [PubMed: 17170295]

NASA Author Manuscript

NASA Author Manuscript

NASA Author Manuscript

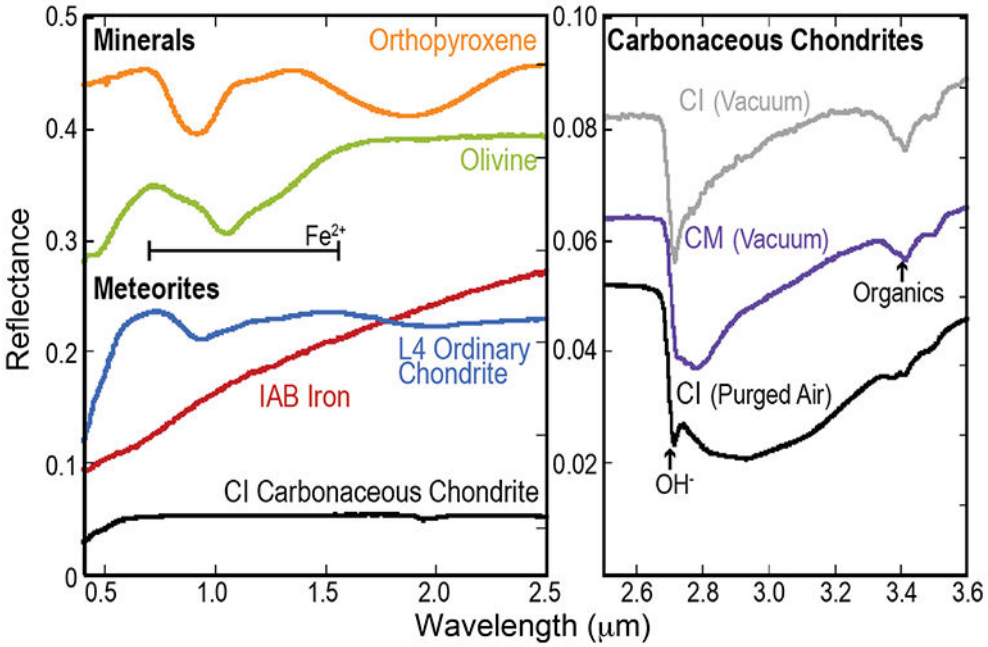

Fig. 1.

Example of silicate, carbonate, organic, and accessory mineral spectral features in the near IR region. Data sourced from Takir et al. (2013), McAdam et al. (2015), and the RELAB database.

NASA Author Manuscript NASA Author Manuscript NASA Author Manuscript

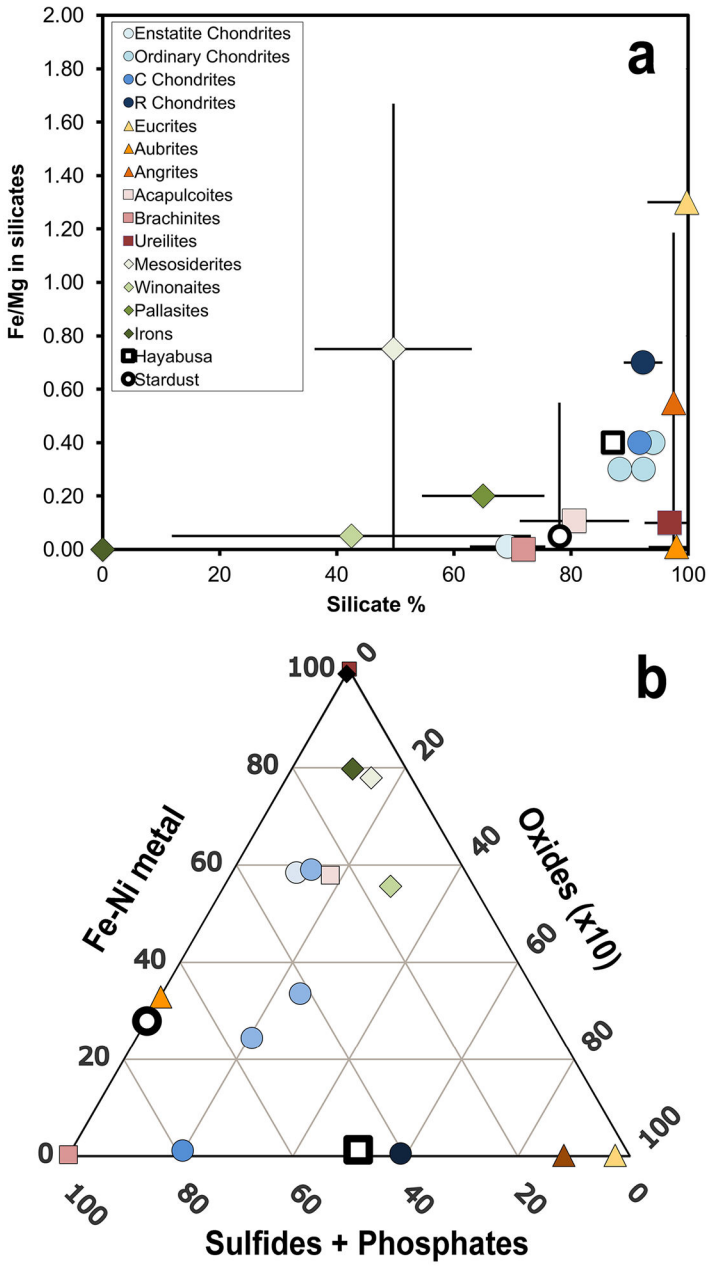

Fig. 2.

Meteorite groups plotted as simple combinations of (a) silicate abundance and Fe/Mg ratio in the silicate fraction (unequilibrated meteorites have large ranges in Fe/Mg ratios) and (b) sulfides + phosphates, oxides, and Fe-Ni metal.

NASA Author Manuscript

NASA Author Manuscript

NASA Author Manuscript

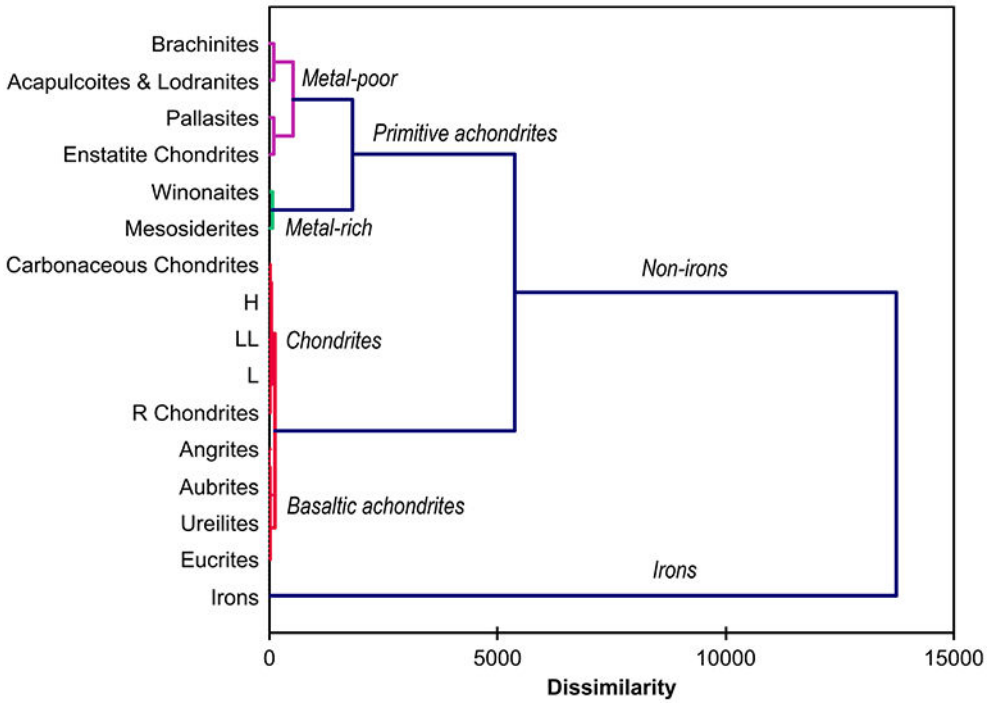

Fig. 3.

Dendrogram showing the results of agglomerative hierarchical clustering of meteorite classes in Table 1 using only the average abundance of four mineral phases (silicate, sulfides + phosphates, oxides, and Fe-Ni metal). Each merge is represented by a horizontal line. The distance along the *x*-axis represents the similarity of the clusters that were merged. In general, multidimensional fitting using these parameters distinguishes major groups of meteorites from each other.

NASA Author Manuscript NASA Author Manuscript NASA Author Manuscript

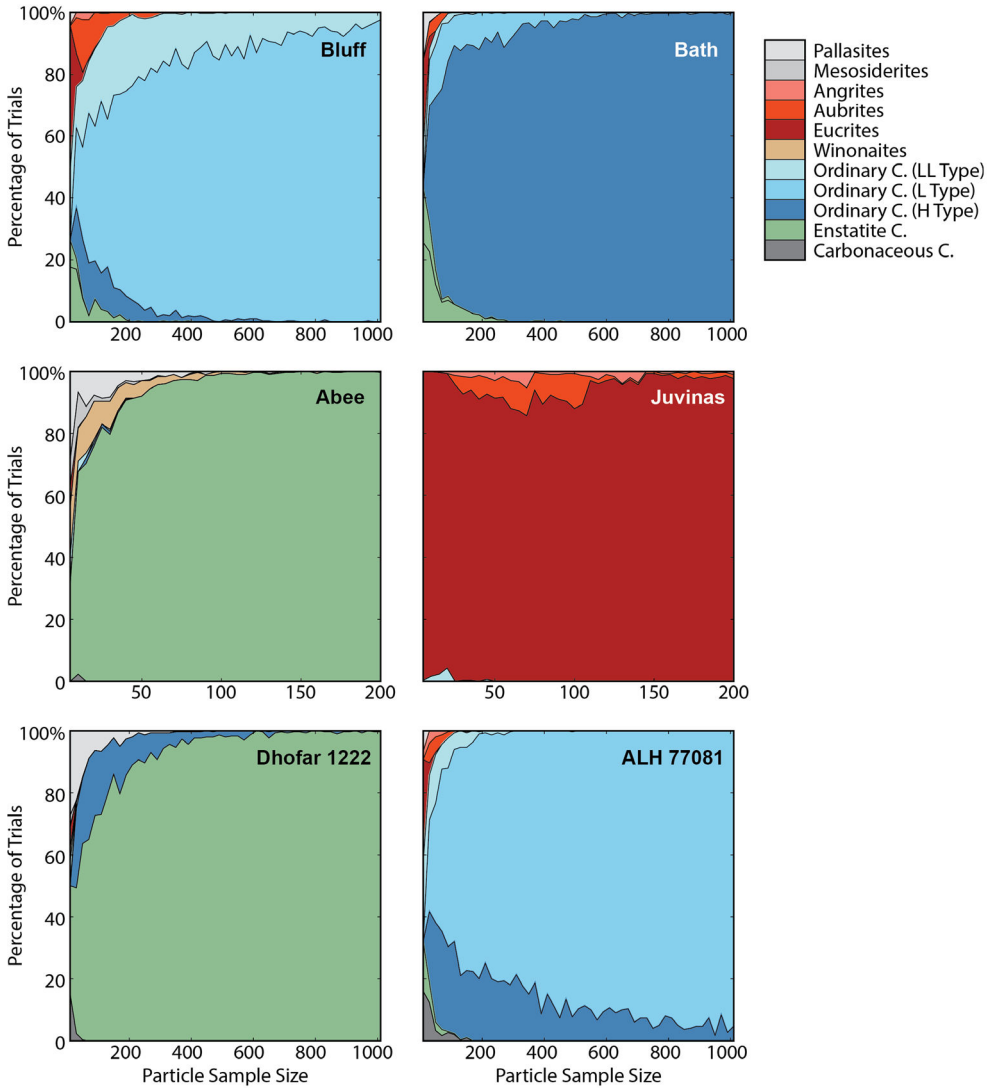

Fig. 4.

Classification results for model data sets created from known meteorites. Bluff and Bath are linked to ordinary chondrites in about 100 samples, and to their subclass in about 200 samples. Abee and Juvinas are shown to be an enstatite chondrite and a eucrite using only tens of samples. However, metal-poor acapulcoites Dhofar 1222 and ALH 77081 are confused with other classes.

NASA Author Manuscript NASA Author Manuscript NASA Author Manuscript

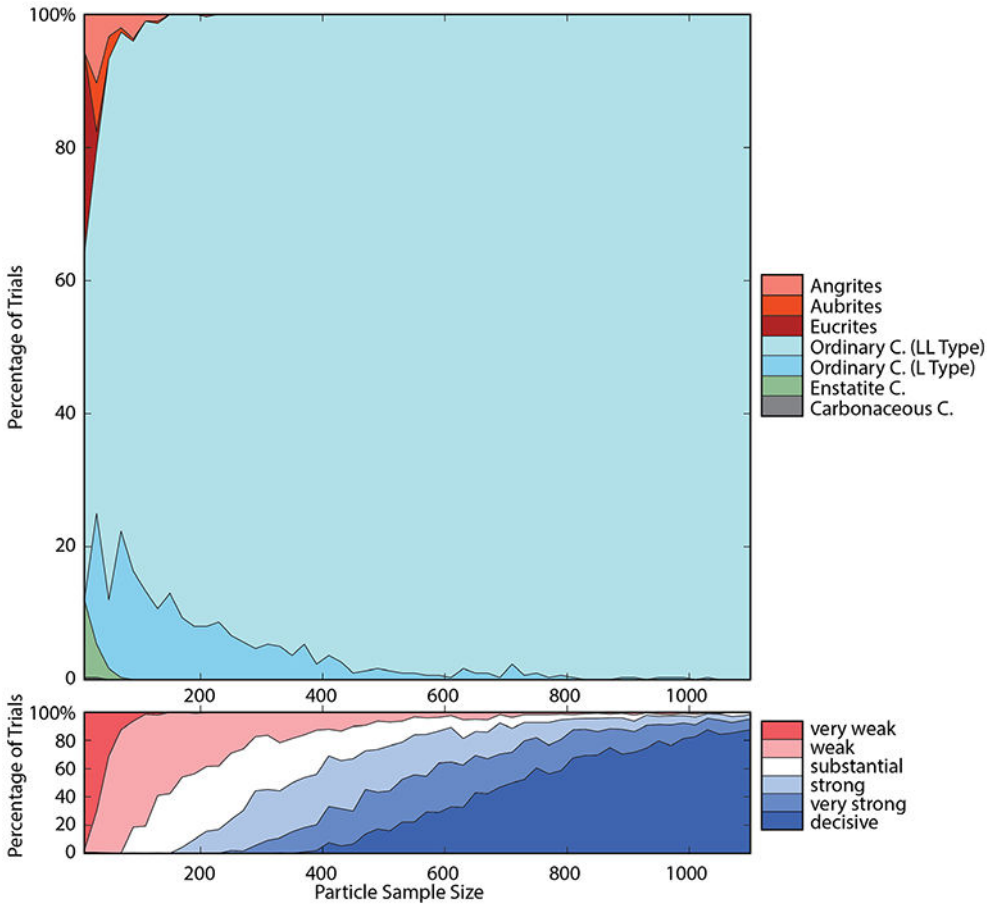

Fig. 5.

Top) Selected meteorite classes for individual trials (*y*-axis) of sample sets with *n* from 20 to 1100 (*x*-axis) selected from the Hayabusa returned sample (Table 1). As *n* increases, the number of trials corresponding to chondrites, and specifically LL-chondrites, increases. Bottom) The evidential strength of the selected meteorite class for each individual trial, no matter the guessed type. For small numbers of particles, the evidence to suggest that the sample matches one meteorite class over another is generally weak, but increases with increasing *n*.

NASA Author Manuscript

NASA Author Manuscript

NASA Author Manuscript

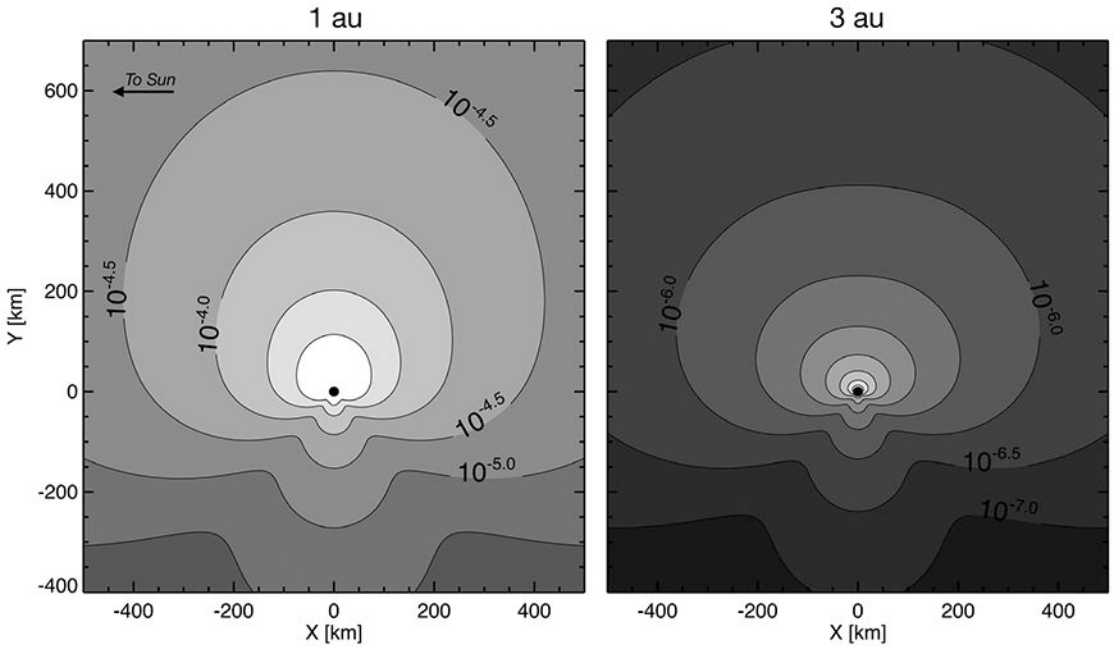

Fig. 6.

Comparison of the ejecta cloud structure, in particles per m^3, for a 10 km radius body at 1 and 3 au for grain radii $a > 50$ nm. The reference frame shown has the Sun fixed in the $-x$ direction and the apex direction in the $+y$ direction. Due to the expected larger decrease in retrograde HTC particles compared to JFCs producing the HE/AH ejecta, ejecta from the apex source is reduced at 3 au producing a flattened density distribution.

NASA Author Manuscript NASA Author Manuscript NASA Author Manuscript

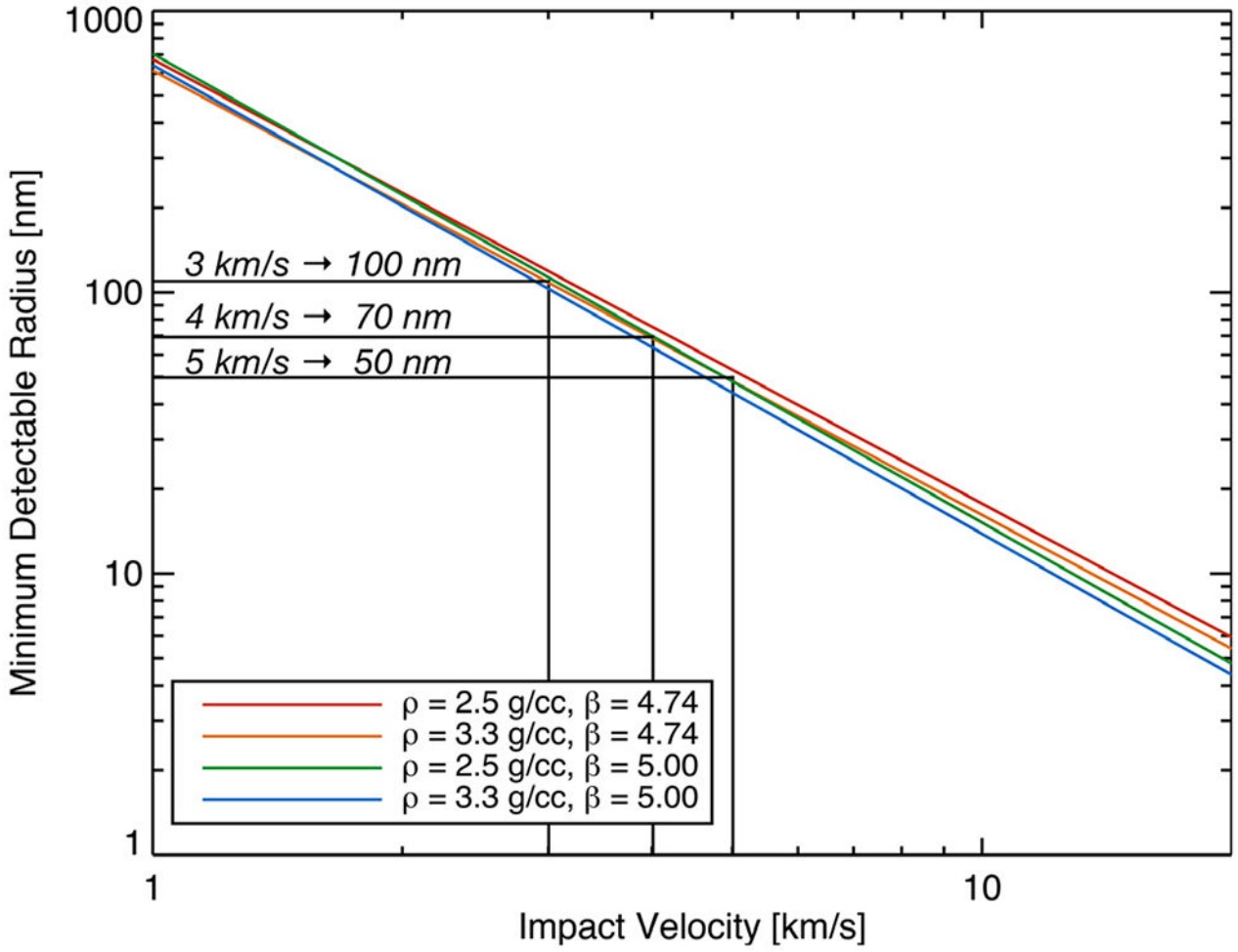

Fig. 7.
Minimum detectable dust grain radius as a function of impact velocity.

NASA Author Manuscript

NASA Author Manuscript

NASA Author Manuscript

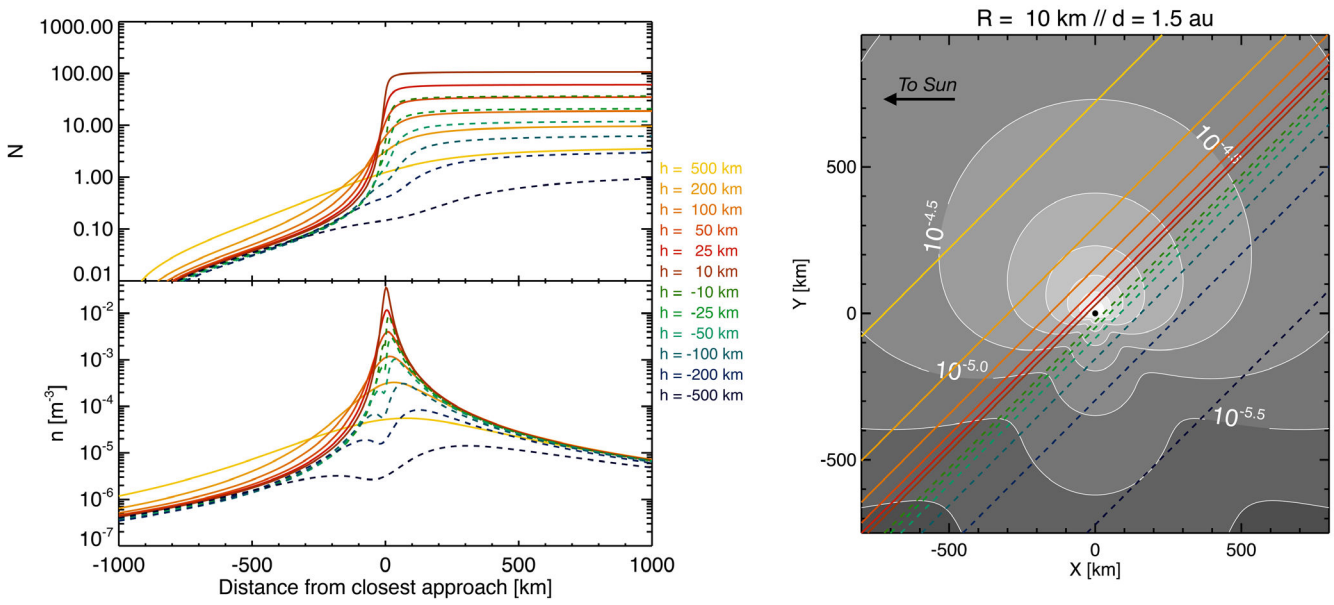

Fig. 8.

Total number of impacts and predicted dust density ($a > 50$ nm) for a 10 km radius body at 1.5 au. Contours are logarithmically spaced in units of 10^{-3} m^{-3}.

NASA Author Manuscript

NASA Author Manuscript

NASA Author Manuscript

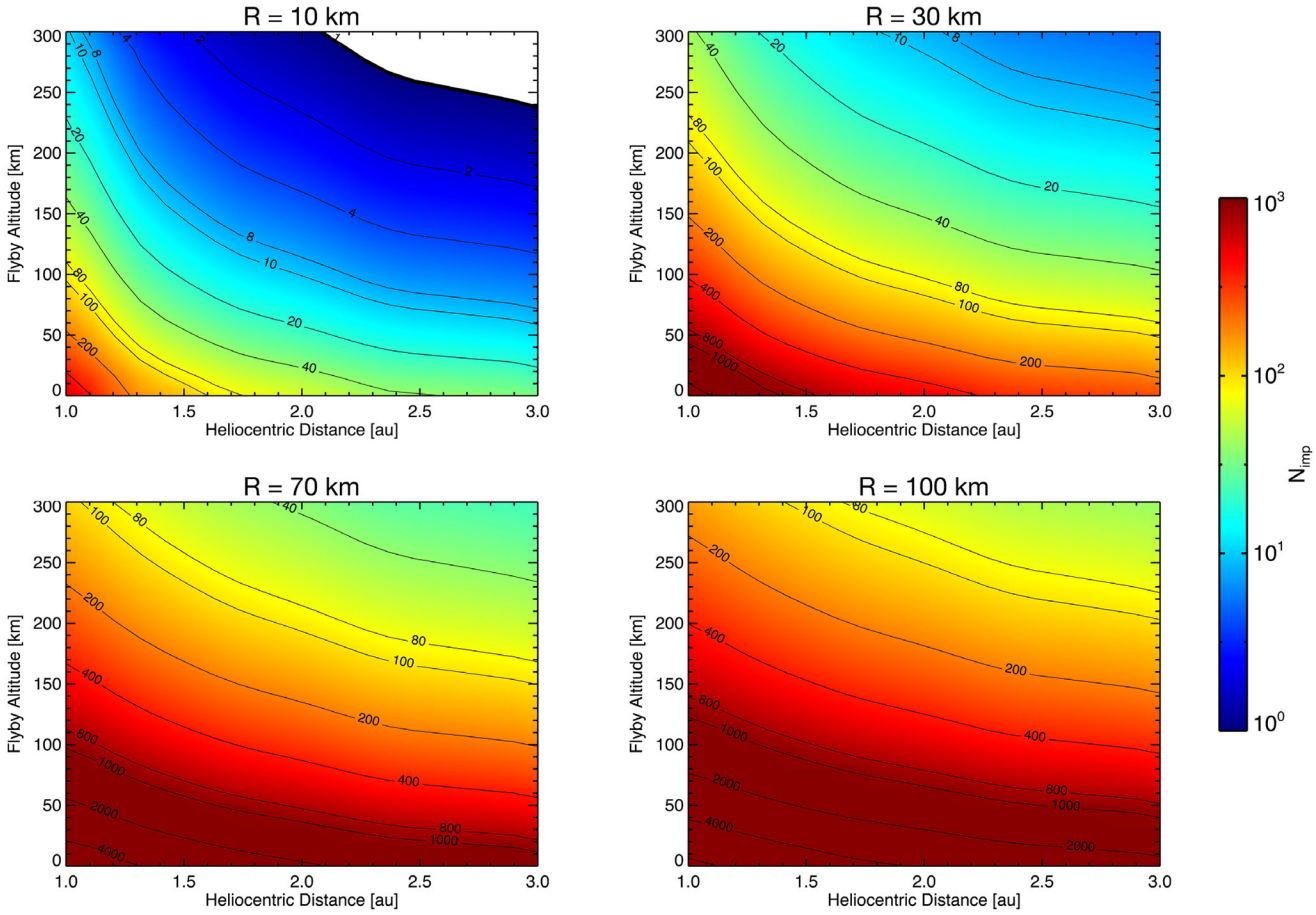

Fig. 9.

Total impact count predictions for grain size a >50 nm as a function of heliocentric distance and flyby altitude for R = 10, 30, 70, and 100 km.

NASA Author Manuscript

NASA Author Manuscript

NASA Author Manuscript

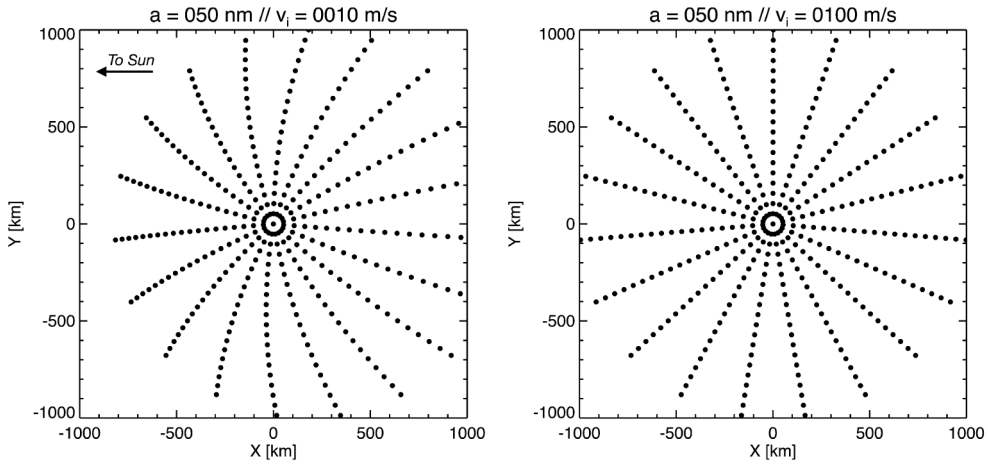

Fig. 10.

Simple simulation showing the effects of radiation pressure on ejecta dynamics, with the dots representing positions of grains launched from the surface at different times. Left and right are given for initial speeds of 10 and 100 m s^{-1}, respectively.

NASA Author Manuscript NASA Author Manuscript NASA Author Manuscript

Meteorit Planet Sci. Author manuscript; available in PMC 2020 April 03.

Table 1.

Asteroid classes and linked meteorite groups and their mineralogical characteristics.

Class	Group	Asteroid match	Silicate Fe/Mg ratio	Silicate (%)	Sulfides and phosphates (%)	Oxides (%)	Fe-Ni metal (%)	Carbon-bearing phases	Hydrous phases	Reference
Enstatite	E	M	0.01 ± 0.01	69.2 ± 6.5	10.5 ± 4.1	–	20.3 ± 7.1	x	x	Keil (1968)
Ordinary	H	S	0.3	88.3 ± 1.2	3.7 ± 0.8	0.2 ± 0.1	7.9 ± 0.8			Keil (1962)
	L		0.3	92.4 ± 1.2	4.1 ± 06	0.2 ± 0.1	3.3 ± 1.1			
	LL		0.4	94.0 ± 1.0	4.1 ± 0.8	0.2 ± 0.1	1.8 ± 0.6			
Carbonaceous	Many	C (D, B, F, G, Q)	0.4	93.1 ± 11.3	0.5	0.2	5.4 ± 7.1	x	x	Bland et al. (2004)
Rumuruti	R	None identified	0.7	92.3 ± 3.3	5.4 ± 3.0	0.8 ± 0.6	0.1 ± 0.1		Trace	Kallemeyn et al. (1996)
Basaltic achondrites	Eucrites	V	1.3 ± 0.5	99.8 ± 6.7	0.3 ± 0.2	0.9 ± 0.6	–			Mayne et al. (2009)
	Aubrites	E	0.01 ± 0.01	98.0 ± 4.8	1.7 ± 2.7	–	0.8 ± 1.4			Mittlefehldt et al. (1998)
	Angrites	None identified	0.6 ± 0.6	97.5 ± 0.7	1.2 ± 0.1	0.9 ± 0.3	–			Bischoff et al. (2000); Jambon et al. (2005)
Primitive achondrites	Acapulcoites and Lodranites	None identified	0.11 ± 0.04	80.5 ± 9.3	4.5 ± 4.0	0.3 ± 0.4	10.5 ± 9.4	x	x	Rubin (2007)
	Brachinites	None identified	1–2	71.9 ± 40.3	3.1 ± 2.1	–	–	Mittlefehldt et al. (1998)		
	Ureilites	None identified	0.3 ± 0.1	96.8 ± 4.3	–	–	1.3 ± 0.6	x		Singletary and Grove (2003)
Metal-rich	Mesosiderites	(S) (V)	0.8 ± 0.9	49.6 ± 13.4	4.1 ± 3.4	0.8 ± 0.4	43.4 ± 18.9			Mittlefehldt et al. (1998)
	Winonaites and silicate-bearing irons	(M)	0.1	42.5 ± 30.6	10.8 ± 13.7	2.1 ± 3.5	40.2 ± 28.4	x		Mittlefehldt et al. (1998)
	Pallasites	A	0.2	65.0 ± 10.4	3.8 + 2.6	0.4 ± 0.5	30.8 ± 9.6			Buseck (1977)
	Irons	M	–	–	<1	–	~100	x		
Missions	Hayabusa	S	0.4	87.2	11.3	1.2	0.3			Nakamura et al. (2012)
	Stardust	–	0.5 ± 0.5	58.8	14.7		5.9	x		Zolensky et al. (2006)

NASA Author Manuscript

NASA Author Manuscript

NASA Author Manuscript

Table 2.

Threshold values and adjectival ratings of likelihood ratio (LR).

LR value	Adjectival strength
$LR > 10^2$	Decisive
$10^{1.5} < LR < 10^2$	Very strong
$10^1 < LR < 10^{1.5}$	Strong
$10^{0.5} < LR < 10^1$	Substantial
$10^0 < LR < 10^{0.5}$	Weak
$LR < 10^0$	Very weak

NASA Author Manuscript NASA Author Manuscript NASA Author Manuscript

Table 3.

Test case meteorite phase abundances, most likely model classification, and number of particles *n* in the sample required to yield the most likely class (and subclass) in 90% of trials. In general, tens to hundreds of particles are sufficient to classify a sample using only these parameters; however, in some cases, additional information would be useful.

Meteorite	Class	Silicate Fe/Mg	Silicate	Sulfides + phosphates	Oxides	Fe-Ni metal	Model class (subclass)	*n*
Bluff	L5	0.25	92.2	4.2	0.36	3.2	Ordinary chondrite (L)	100 (200)
Bath	H4	0.30	88.8	3.6	0.09	7.5	Ordinary chondrite (H)	100 (200)
Abee	Enstatite	0.02	58.8	17.4	0.00	23.8	Enstatite	50
Juvinas	Eucrite	1.57	99.1	0.2	0.70	0.0	Eucrite	20
ALH A77081	Acapulcoite	0.12	88.2	5.2	1.30	4.4	Ordinary chondrite (L)	100 (700)
Dhofar 1222	Acapulcoite	0.07	73.8	6.4	0.30	16.5	Enstatite	200
Hayabusa	LL5						Ordinary chondrite (LL)	100 (200)